TRITA-ALF 92:03
ISSN 1102-2051
ISRN KTH/ALF/R--92/3--SE

TRITA-ALF--92-03

Reversed Field Pinch Magnetic Equilibrium and Profile Dynamics in Extrap T1-Upgrade

P. Nordlund, S. Mazur and J.R. Drake

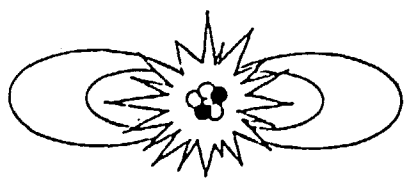

Research and Training programme on
CONTROLLED THERMONUCLEAR FUSION
AND PLASMA PHYSICS (EUR-NFR)

FUSION PLASMA PHYSICS
ALFVÉN LABORATORY
ROYAL INSTITUTE OF TECHNOLOGY
S-100 44 STOCKHOLM SWEDEN

Reversed Field Pinch Magnetic Equilibrium and Profile Dynamics in Extrap T1-Upgrade

P. Nordlund , S. Mazur and J.R. Drake

Stockholm, May 1992

Department of Fusion Plasma Physics
Alfvén Laboratory, Royal Institute of Technology,
S-100 44 STOCKHOLM,Sweden

Reversed Field Pinch Magnetic Equilibrium and Profile Dynamics in Extrap T1-Upgrade

P. Nordlund, S. Mazur and J.R. Drake

Abstract

An eight station insertable magnetic probe has been installed on the Extrap T1-U machine. The structure of the Reversed Field Pinch magnetic equilibrium and the time evolution of the profiles has been studied. The probe was inserted into sustained high current density RFP plasmas, typically 12-16 MA/m^2 on axis. When the probe was inserted there was a somewhat shorter pulse duration and a slightly decaying current. The magnetic field profiles are shift corrected and expressed in a cylindrically symmetric form. All quantities are then derived from cylindrically symmetric equations. In the beginning of the sustainment phase, where the best reproducibility is achieved, we have been able to resolve in estimates of the pressure profile consistent with independent measurements of the radial pressure. Values of $\beta_\theta \approx 0.19$ and $< \beta > \approx 0.09$ are found leading to an estimation of the energy confinement time, with the probe inserted, of $\tau_E \approx 5$ μs.

Profiles of the effective parallel conductivity clearly indicates the presence of a "dynamo mechanism" sustaining the field configuration. High Θ discharges usually exhibit large oscillations in the F-Θ plane. We find that these oscillations represents macroscopic redistribution of the current in the plasma. A cyclic process is found where the parallel current density (μ–profile) tends to peak in the center and then relax towards a flatter and broader configuration. Towards the end of the discharge there is an increasing fluctuation level along with an increasing V_{loop}/ I_p. Here we find a relative increase in the current density in the edge region resulting in a hollow μ–profile.

CONTENTS

1. INTRODUCTION

The RFP magnetic field configuration represents a near minimum energy state to which the plasma spontaneously relaxes. Experimentally RFPs are sustained well beyond the resistive diffusion time. It is found that supplying volt seconds for the poloidal magnetic field sustains the toroidal magnetic field configuration as well. The mechanism responsible for this process is commonly referred to as the "RFP dynamo". Because of their crucial role, magnetic field profiles has been measured in several RFP experiments [1-4]. Recently the time evolution of the profiles have been discussed in terms of a cyclic current redistribution associated with the sustainment of the configuration [5-6].

Reversed Field Pinch (RFP) discharges with very high current density, greater than 15 MA/m^2, are studied in the Extrap T1-Upgrade machine. The device has a distant resistive shell and the high aspect ratio of the machine ($R/a = 8.8$) is rather unique among present day RFP experiments.

In this paper we present a study of the equilibrium profiles and their dynamics during RFP operation in T1-U. Although perturbing, insertable magnetic probes are really the only way to obtain detailed information about the magnetic field profiles and their evolution during the discharge.

In section 2. the experimental setup is described. The results are in general quite sensitive to experimental errors in the magnetic field profiles. In this perspective the construction of the probe and the techniques concerning calibration and alignment are described in some detail. The propagation of errors is discussed and a short description of the data acquisition is given. In section 3.2. the equilibrium profiles are presented. The raw field profiles are compensated for their equilibrium flux surface displacements with respect to the geometrical axis and expressed on a cylindrically symmetric form. All quantities are then derived from cylindrically symmetric equations. Estimates of current densities, safety factor and pressure are presented. Section 3.3. deals with the time

evolution of the equilibrium profiles, electric fields and "anomalous" conductivity. In section 4. the results are discussed and compared with observations on other experiments. The conclusions are given in section 5.

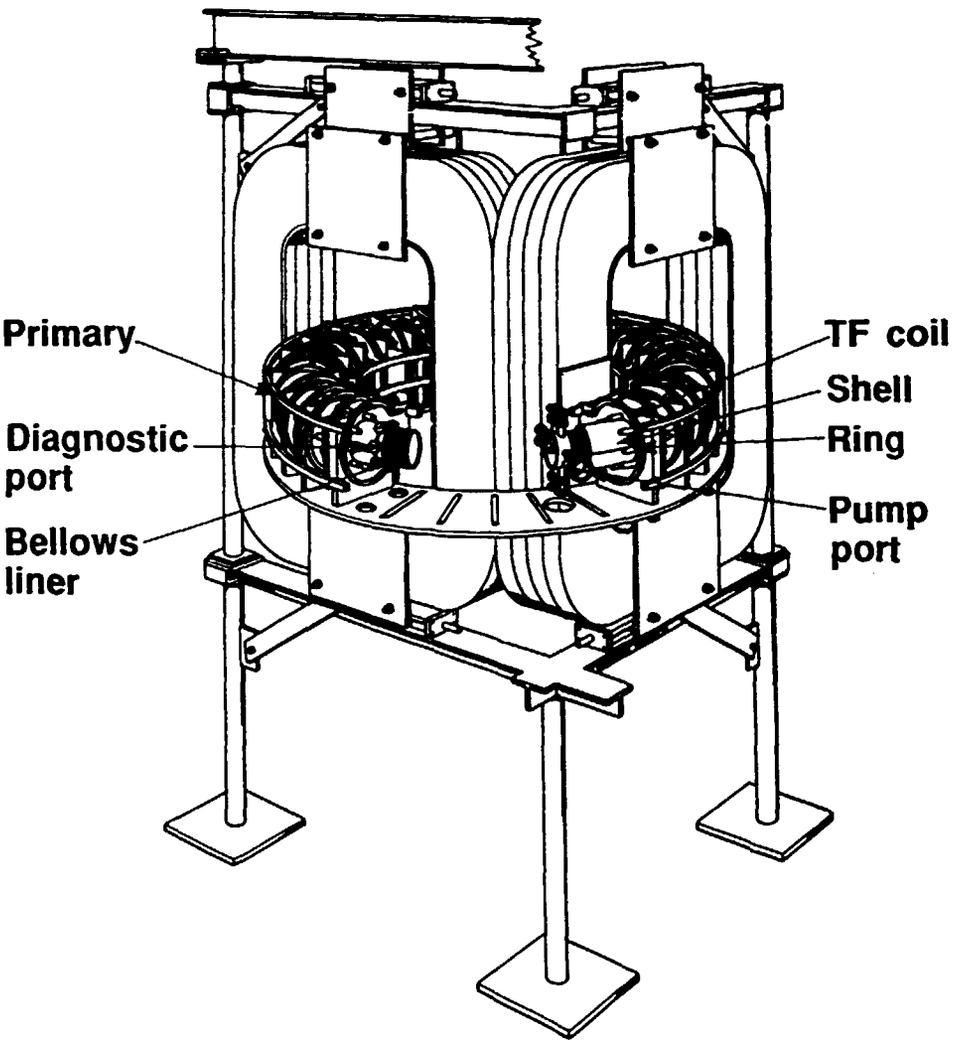

Fig. 1. Schematic drawing of the Extrap T1-Upgrade machine.

2. TECHNIQUES

2.1.The Extrap T1-Upgrade Machine

Extrap T1-Upgrade is a high aspect ratio (R/a = 8.8) toroidal pinch with a distant resistive shell (fig.1). The device has recently been modified and several new diagnostics, including an insertable magnetic probe, have been installed. The modifications involved replacement of the old vacuum vessel, which was contaminated by flourine, improving the plasma boundary conditions by replacing the stainless-steel shell by a thin brass shell with a longer time constant and reduction of field errors by installing additional copper foils at the poloidal gaps in the shell.

The vacuum vessel consists of a thin-walled stainless steel bellows construction with a penetration time of 5 μs for perpendicular fields and 50 μs for the toroidal field. The shell is segmented with 12 poloidal gaps and two toroidal gaps on the inboard and outboard side of the equatorial plane (thus the shell does not conserve toroidal flux). The resulting average field penetration times are about 300 μs for the radial field and 500 μs for the vertical field respectively. The vacuum region between the plasma boundary and the resistive shell is about 16% of the minor radius.

The flux-swing of the iron core is 0.4 Vs. During RFP operation, termination of the discharge usually occurs before core saturation. The current distribution in the eight primary turns of the OHC can be controlled to provide the necessary equilibrium vertical field for pulse lengths in the order of, or longer than the shell penetration time.

For RFP operation a small, low inductive capacitor bank is used to produce the initial toroidal field. After reversal, the toroidal field is sustained by a power crowbar which drives the reversed current for *aided reversal* operation. Furthermore, the voltage over the toroidal field coil is "optimized" to compensate the resistive losses in the TF-coil.

The discharge chamber is pumped by three turbomolecular pumps to ensure a UHV quality vacuum. The base vacuum is typically less than 10^{-8} Torr.

For the experiments described here the plasma current was about 35-50 kA and the filling pressure was in the range of 4 mTorr Hydrogen. Typical parameters of the T1-U experiment are listed in table 1.

Major radius, R	0.5 m
Shell radius, b	68 mm
Limiter radius, a	57 mm
$\tau_{\perp}$ - liner	5 μs
$\tau_{\parallel}$ - liner	50 μs
$\tau_{\perp}$ - shell	300 μs
$\tau_{\parallel}$ - shell	---
Toroidal plasma current, I_p	30 - 80 kA
Rise time of current	100 μs
Pulse duration	up to 1 ms
Electron temperature, T_e	up to 120 eV
Electron density, $<n_e>$	$1 - 2 \times 10^{20}$ m^{-3}

Table 1. Parameters of the Extrap T1-Upgrade machine.

2.2. The Insertable Magnetic Probe

2.2.1. Construction

The insertable magnetic probe consists of an eight station radial array with 10 mm spacing. Each station is comprised of three coils with the same geometric center and nominally orthogonal axes. Thus we are able to simultaneously define the magnetic field in eight equally spaced radial positions. The 24 coils are wound on a graphite former fixed to a carrier which mounted on to a printed circuit board placed in a shielded junction box (fig.2).

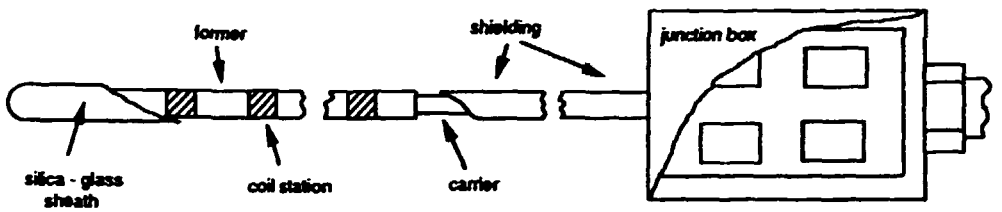

Fig. 2. Schematic drawing of the probe.

To minimize unwanted, nonlocal pick-up of stray signals, the leads are also shielded and connected to the junction box. The coil assembly fits into a quartz sheath with a diameter of 6mm. This protective quartz tube is fused to a rotatable mini Comflat flange which is attached to the probe insertion unit. Copper rings are used to ensure UHV compatibility. The probe insertion unit consists of a translator and a bellows with a full stroke of 160 mm which allows the probe to be inserted into the port on the opposite side of the vacuum vessel. Normally, for equilibrium profile measurements, the probe is inserted so that the first station is centered on the geometrical axis. The whole probe assembly is mounted in a support frame and connected to a port on the outboard side of the torus at an insertion angle of 20 degrees to the vertical axis (fig.3).

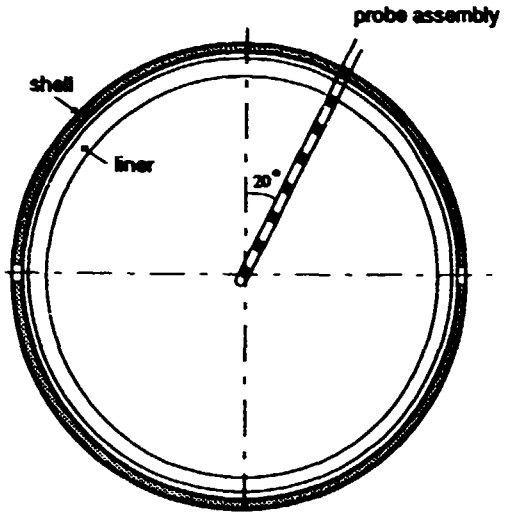

Fig.3. Probe / machine geometry

From the junction box the probe signals are carried to the CAMAC crates by coaxial cables inside an additional copper shielding, again to minimize stray-field pick-up.

2.2.2. Calibration and alignment

In fluctuation measurements, while focusing of the frequency region of interest the equilibrium field and low frequency pick-ups (which are more difficult to get rid of by shielding) are eliminated. Also, generally larger errors are acceptable. But, whenever concerned with quantitative measurements of the equilibrium magnetic field the problem can become quite complicated. A common problem encountered is that of determining a small field component where other components are large. For instance the poloidal field is approaching zero on axis while the toroidal field remain large. Here even a small pick-up of toroidal field could alter the measured poloidal field profile near the axis and thereby introduce false features in the derived quantities. In particular the pressure profile is directly related to perpendicular current density which is relatively small in low β plasmas. In other words the plasma pressure affects the field profiles only very slightly and therefore pressure estimates are very sensitive to experimental errors in the magnetic field

measurements. We shall now discuss the most important sources of error and the methods adopted in eliminating them. The four main types of error that can arise in probe measurements are:

1. Non local contributions to the signals due to pick-up in the leads.
2. Incorrect number of area turns of the individual coils.
3. Relative angular misalignment between the individual coils in the array.
4. Angular misalignment of the probe array with respect to the plasma coordinate system.

The problem of non local pick-up must be treated by shielding and distance, i.e. keeping the transmission cables as far as possible from sources of magnetic field. Concerning the coil areaturns, given the fine scale geometry of the coil former it is clear that we must expect the area turns for the individual coils to differ somewhat from their nominal values. Furthermore, the relative alignment between the coils in the probe array is not perfect. This means that each coil will, in addition to the nominal field component, measure contributions from the other field components. However, if the coil array is inserted into three orthogonal magnetic fields of known strength these problems may be eliminated into a resulting calibration matrix. Once this is done the true magnetic field at each station can be evaluated as the measured field times the inverted calibration matrix for that station:

$$\begin{pmatrix} B_1 \\ B_2 \\ B_3 \end{pmatrix} = \begin{pmatrix} \alpha_{11} & \alpha_{12} & \alpha_{13} \\ \alpha_{21} & \alpha_{22} & \alpha_{23} \\ \alpha_{31} & \alpha_{32} & \alpha_{33} \end{pmatrix}^{-1} \begin{pmatrix} B_1^m \\ B_2^m \\ B_3^m \end{pmatrix} \qquad (2.1)$$

Where α_{ij} are the measured effective area turns for coil i in field j.

To determine the relative misalignment of the different coils in the probe, the probe was calibrated using a Helmholtz coil. A special calibration rig was made where the probe could be inserted into the Helmholtz coil from two directions, along the magnetic field and across the field to the region of greatest field uniformity. When inserted across the field the probe could be rotated 90 degrees with good accuracy. In this manner we were able to

create three orthogonal magnetic fields. With this equipment we where able to calibrate the probe coils to an accuracy better than 97% (fig.4).

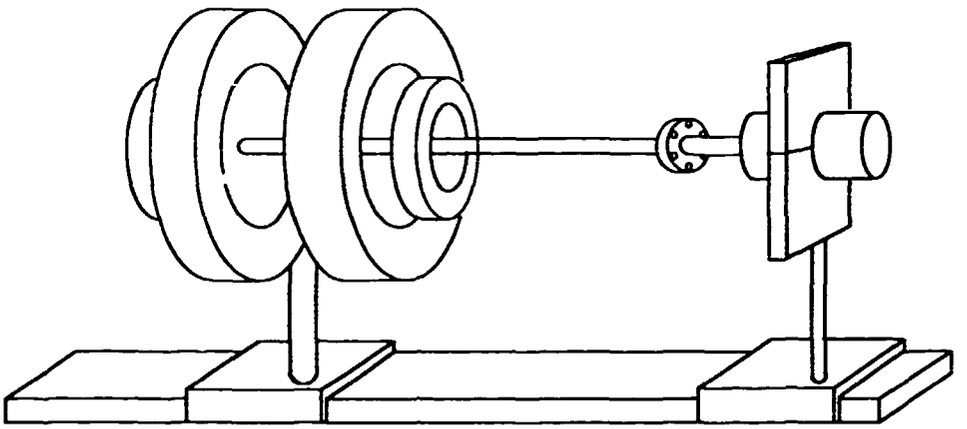

Fig.4. Calibration set up.

Since the plasma coordinate system is determined by the machine geometry, such as the shell, vacuum vessel and coil systems, it is also necessary to determine the orientation of the probe relative to the machine. After a laser guided optical alignment the vacuum magnetic fields, on the geometrical axis of the vessel, where used to determine the remaining misalignment angle of the probe assembly relative to the coordinate system of the machine. In this way we were able to reduce the alignment errors well below 2%. Thus the total systematical errors (i.e. calibration and alignment) could be limited to 4%.

An error propagation analysis for systematic errors is presented in appendix A. Here the calibration matrix is randomly perturbed by systematical calibration errors uniformly distributed between -4% and +4%. We find that the stochastical errors tend to diminish when fitting polynomials to time averaged data from several shots. As for the propagation of systematical errors the most sever error occurs in the pressure profile, about 34 % on axis. The error bars drawn in the plots in section 3.2. are calculated as the standard deviation from the best estimates, calculated for 10 random perturbations of the initial unperturbed calibration matrix, as described in appendix A.

2.3 Data acquisition

The probe data is recorded using a CAMAC data acquisition system. The signals are connected via variable attenuators to active integrators with an integration constant of 100 μs. Integrated signals are recorded using AEON 3248 transient recorders. The transient recorders digitizes 1024 samples during one shot with a resolution of 8 bits and a sampling frequency of 0.25 - 10 MHz. Recorded data is stored on a LSI11/73 computer using the CAMAC software DAMPT. Data for the shots used in the analysis is moved to a Micro-Vax 3400 where the raw data is stored.

Software for analysis and display of the probe data is written in IDL (Interactive Data Language) on a Vax-station VLC 4000 where the analysis is performed. IDL is a software system for the interactive analysis and display of scientific data. The software package includes libraries with both graphical and mathematical routines.

3. RESULTS

3.1 Global performance

The probe was inserted into RFP discharges with plasma currents in the range of 30 - 50 kA and a pulse duration of 500 μs. In fig.5 we show a comparison of plasma current, loop voltage, average and edge toroidal fields between a shot with the probe retracted and a shot with the probe inserted. The two shots have the same external circuit programming and the same filling pressure, about 4 mTorr. When the probe was inserted there was an increase in the power input and a somewhat shorter pulse duration. However there was still a clear drop in the loop voltage around field reversal and VUV spectroscopy indicated burn-through of low Z impurities. The average and edge toroidal field remained essentially unchanged while there was a slightly decaying current in the probe discharges. Both discharges terminated in a similar manner. The cause of the termination is not clear, however a gradual upward drift of the plasma column is observed by external equilibrium diagnostics as well as with the probe. The typical discharge duration is slightly longer than the average magnetic field penetration time of the shell.

Measurements of the line integrated electron density with an interferometer showed a similar behavior with an initial density roughly equal to the filling pressure followed by a pump out during reversal and saturation during the sustainment phase around 10^{20} m^{-3}. Spectroscopic measurements of the electron temperature from line ratios of O^{+5} in the in the VUV region [7], indicate $T_e \approx 55$ eV. External measurements of the magnetic fluctuations measured with edge coils in the interspace between the liner and the shell show a slightly higher activity with the probe inserted.

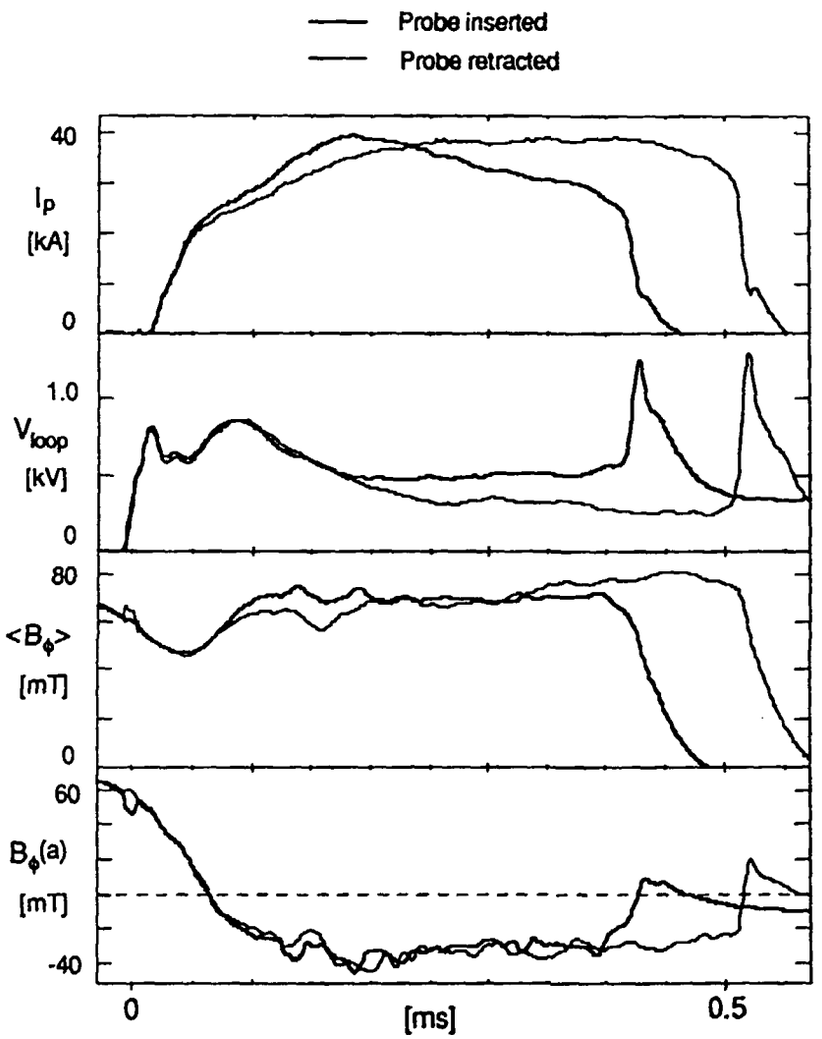

Fig. 5. Global performance of perturbed and unperturbed RFP discharges.

The RFP discharges, obtained so far in T1-U, tend to evolve to relatively deeply reversed high theta discharges (F=-0.4, Θ =1.8). Such discharges exhibit macroscopic oscillations in the F-Θ plane (fig.6). These oscillations appear to be similar to those of unperturbed high-Θ discharges. As will be shown later in this section the probe measurements indicate that the F-Θ oscillations result from macroscopic redistributions of the current in the plasma.

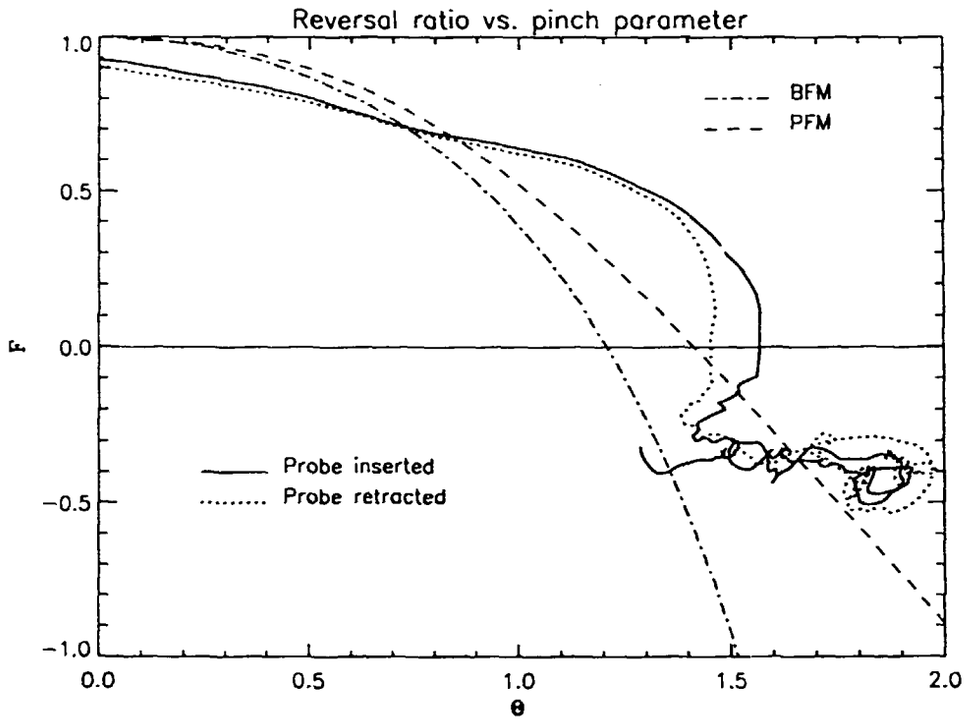

Fig. 6. F-Θ trajectories for the shots in fig.5. The force-free Taylor state (BFM) and the semi-empirical Polynomial Function Model [10] are included for reference.

3.2. Equilibrium Profiles

3.2.1 Raw Magnetic Field Profiles

With the probe inserted over the full minor radius we are able to simultaneously measure the magnetic field as a function of time and radius at eight radial positions. In deriving the long term mean field profiles we find it useful to average over several shots and time windows. In fig.7 we show the raw mean profiles of the toroidal, poloidal and radial magnetic fields for a series of 10 typical RFP discharges in T1-U. Here the the probe has been shifted 5mm radially resulting in field measurements at sixteen points over the radius. This also has the advantage that the remaining systematical errors tend to cancel. The raw data for the individual shots have been averaged over a time period of 60

μs in the beginning of the sustainment phase. The data points are then averaged at each radial position and connected by cubic spline fits.

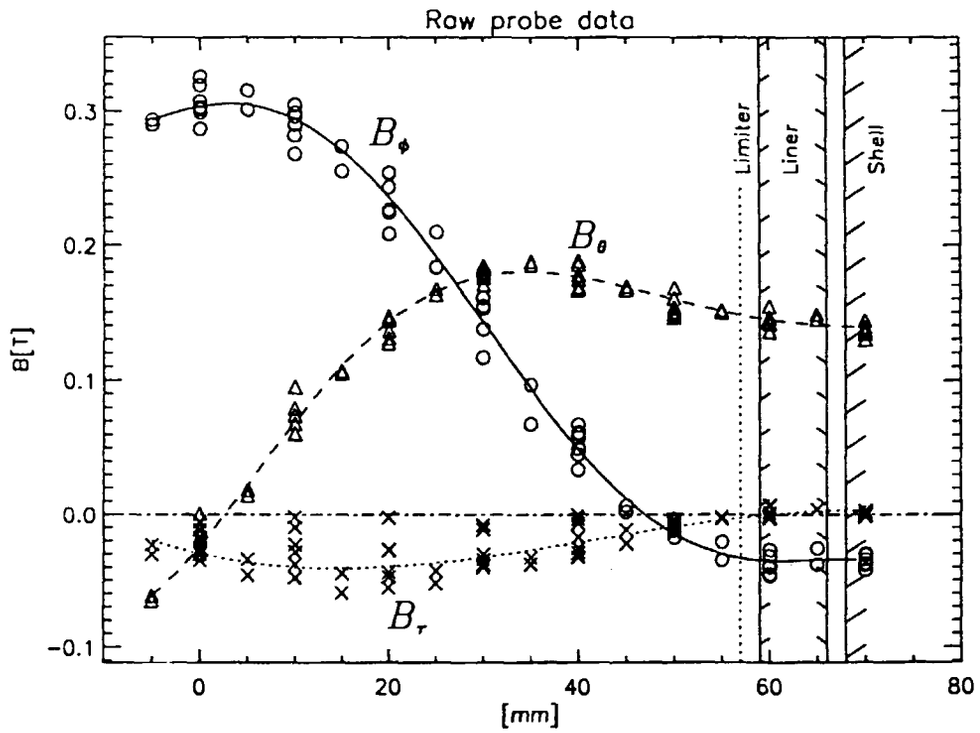

Fig.7. Raw magnetic field profiles.

An important contribution to the scatter in the raw probe data is the different equilibrium displacements of the individual discharges. Note that some of the raw data points in fig.7 are located in the port. Here the magnetic field is perturbed by asymmetric currents in the port section. Before fitting polynomials to the data, these points will be replaced by complementary measurements of B_θ and B_ϕ by edge coils. While these additional data points are adequate for the long term mean field profiles during the sustainment phase where the liner current easily can be subtracted, this technique cannot be used in the analysis of the profile dynamics. This is because the edge coils are not situated at the same location as the probe. Even if they where, the interpretation of dynamics on time scales shorter than, or in the order of the penetration times of the liner would be complicated.

3.2.2. Displacement of Flux Surfaces

The most convenient way to proceed with the analysis of the probe data is to express the profiles in a cylindrical system. In this way the results may be derived from cylindrically symmetric equations. To achieve this goal we must correct for the displacement of the flux surfaces. If this is not done properly we would expect false features to appear in the results, particularly in the pressure profile.

The probe is inserted into the discharge vessel at an angle of 20 degrees to the vertical axis. This means that the flux surfaces will, in general, be displaced both parallel and perpendicular to the probe array. In the following analysis we shall assume circular flux surfaces (for reasons of symmetry). Furthermore we shall assume the parallel displacement $\delta_{\parallel}(r)$ to have the same spatial dependence as the perpendicular displacement $\delta_{\perp}(r)$, or equivalently that the centra of the displaced flux surfaces lie on a straight line as in fig. 8.a.

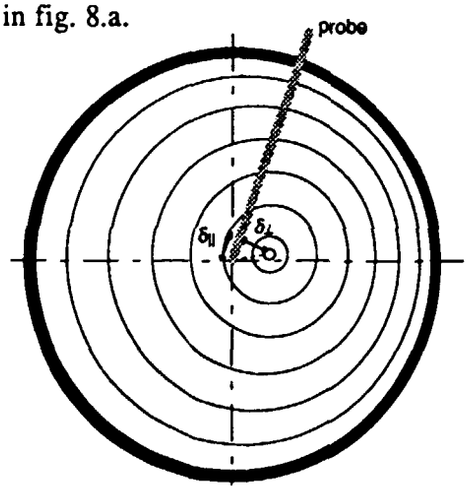

Fig. 8.a.

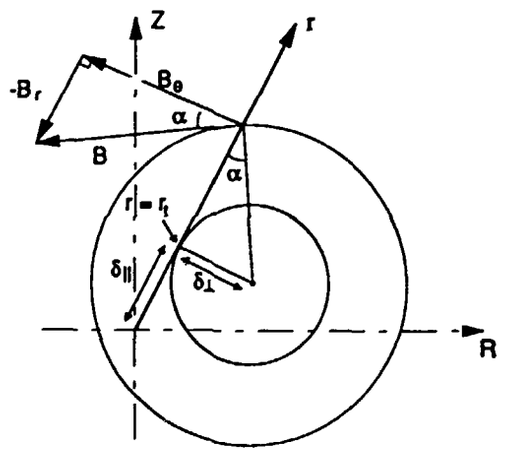

Fig. 8.b.

From fig.8.b. it is evident that $\delta_{\perp}(r)$ can be calculated from the radial and poloidal fields as:

$$\delta_{\perp}(r) = (r - \delta_{\parallel}(r)) \frac{-B_r(r)}{B_\theta(r)} \qquad (3.1)$$

It is also clear (fig.8.b) that we are only able to measure $\delta_{\parallel}$ at the flux surface tangenting the probe ($r = r_t$ in fig.8.b). Note that $\delta_{\perp}(r)$ is quite insensitive to the shape of

$\delta_{\parallel}(r)$ (r_t is known and $\delta_{\parallel} << r$ in the edge region). Instead, the shape of $\delta_{\parallel}(r)$ is important when correcting for the parallel flux surface displacements before fitting polynomials to the data. To determine the form of $\delta_{\parallel}(r)$ we now proceed in the following manner. $\delta_{\parallel}(r)$ is taken to have the form:

$$\delta_{\parallel}(r) = r_t \left(1 - \frac{|(r-r_t)|^{\gamma}}{|(a-r_t)|}\right) \qquad (3.2)$$

where different values of the exponent γ are tried until $\delta_{\parallel}(r)$ shows the same spatial form as $\delta_{\perp}(r)$, calculated from eq. (2). The result of this procedure is shown in fig.9.

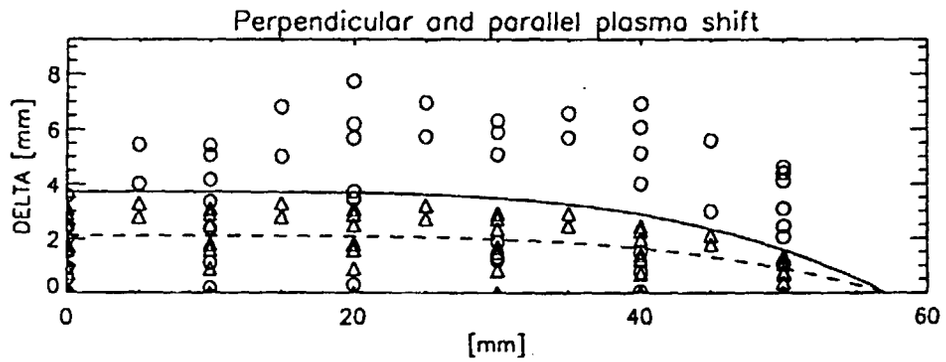

Fig.9. Profiles of the parallel (dashed curve) and perpendicular (solid curve) flux surface displacements

A "match" was found for $\gamma = 6$. The scatter in the calculated displacement is mostly due to the small alignment errors in the radial coils which then pick up the much stronger poloidal and toroidal field components. Note that the plasma takes on the form of a uniformly shifted equilibrium in the central region of the discharge.

The chosen form of $\delta(r)$ implies that $\delta(a)$ is zero. In other words this means that the outermost closed plasma flux surface is centered within the liner. This can be achieved by means of an optimized vertical field [8].

3.2.3. Shift Corrected Field Profiles

Because of the high aspect ratio and the fact that the probe is inserted 20 degrees to the vertical axis, the toroidal effects are quite small. Nevertheless, the toroidal and poloidal field profiles are compensated for the 1/R dependence. As we have shown in 3.2.2. the equilibrium may be characterized essentially by a set of concentric flux surfaces. Accordingly, $B_\theta \propto 1/R$ where R is the major radius.

To correct for the parallel displacement we now define a new radial coordinate along the probe r*, originating at the radius where the measured B_θ equals zero .

$$r^* = r - \delta_{||}(r) \qquad 0 \leq r^* \leq r_{shell} \tag{3.3}$$

Since $\delta_{||} = 0$ outside the liner radius, as discussed above, r* is equal to r in this region.

Expressing the radial coordinates for the measured data in r*, polynomials of typically tenth order are fit to the probe data using a least squares fit.. Terms with odd exponents are fitted to the poloidal field and terms with even exponents to the toroidal field. As mentioned above additional data calculated from external coils in the interspace between the liner and the shell are used to weight a vacuum field configuration from the limiters outwards. This is accomplished by including extra points calculated from the edge coils, with a 1/r dependence for B_θ and a constant value for B_ϕ. Apart from improving the edge fit, this also improves the fit in the center region since it allows polynomials of higher orders to be fitted to the data.

$$B_\theta(r^*) = \sum_{j=0}^{n} a_j \, r^{*\,(2j+1)} \tag{3.4}$$

$$B_\phi(r^*) = \sum_{j=0}^{n} b_j \, r^{*\,2j} \tag{3.5}$$

In fig.10 we plot, as a function of r*, polynomial fits to the toroidal and poloidal

fields together with the measured data points from the probe for the same 10 RFP discharges as in fig.7. The extra points calculated from the external coils are included in the plot.

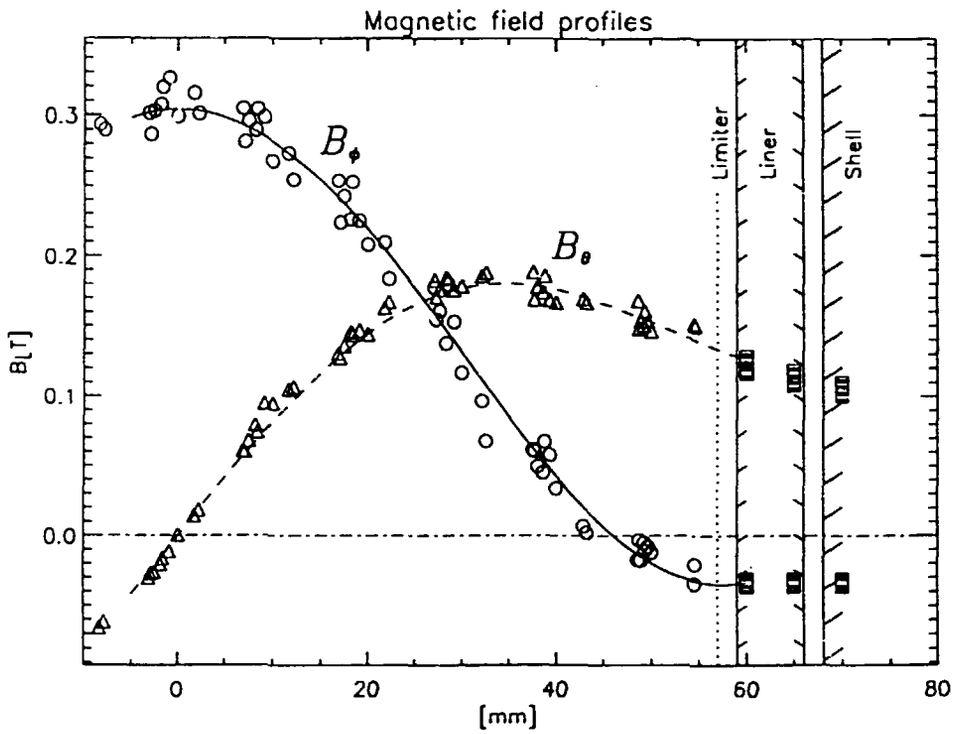

Fig.10. Magnetic field profiles compensated for the parallel shift.

The remaining scatter in the raw data is mainly due to shot to shot variations (no normalization has been done)

Turning to the question of the perpendicular displacement, $\delta_\perp$, it is clear that the field profiles, measured along r^*, must deviate from the profiles in a cylindrical system originating at the magnetic axis. In particular the measured toroidal field at $r^* = 0$ is lower than the value at the magnetic axis. From fig.5. we know that the plasma takes on the form of a uniformly shifted equilibrium in the central region of the discharge. Accordingly we may correct the profiles for a uniform perpendicular shift. This can be done as a correction of the coefficients of the field polynomials in terms of the central perpendicular displacement $\Delta_\perp$ [9].

$$B_\theta(\rho) = \sum_{j=0}^{n} a_j (1 - \frac{j\Delta_\perp^2}{\rho^2}) \rho^{(2j+1)} \tag{3.6}$$

$$B_\phi(\rho) = \sum_{j=0}^{n} b_j (1 - \frac{j\Delta_\perp^2}{\rho^2}) \rho^{2j} \tag{3.7}$$

Here ρ originates at the magnetic axis.

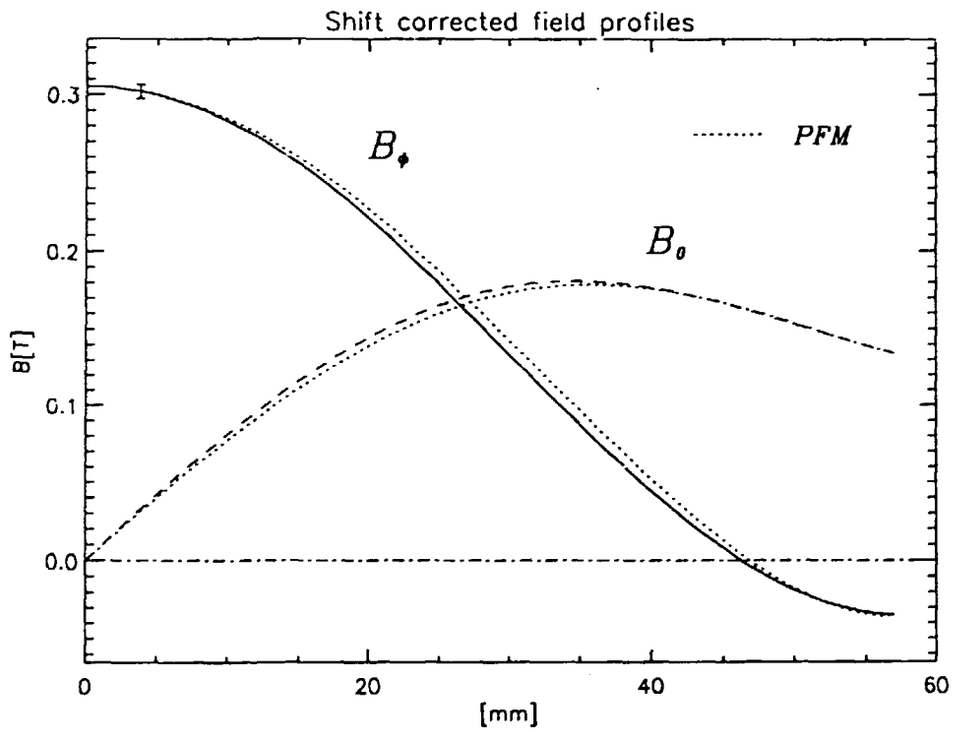

Fig.11. Shift corrected field profiles expressed as a function of a radial coordinate (ρ) originating at the magnetic axis. PFM profiles for Θ = 1.8 are plotted for reference.

Shift correction of the polynomial coefficients for a uniform perpendicular plasma shift is outlined in appendix B. The shift corrected field profiles plotted in fig.11 are obtained by evaluating the polynomials from the corrected coefficients. We note that the resulting pinch parameter (Θ = 1.8) ,calculated from these profiles, agrees within 2% of external measurements.

In addition to the shift corrected field profiles we have also plotted profiles representing the polynomial function model, PFM [10]. The PFM profiles are evaluated for the measured reversal ratio, F, and on axis toroidal field, $B_\phi(0)$, as:

$$B_\phi(\rho) = B_\phi(0)\left(1 - \Theta_0^2\left(\frac{\rho}{a}\right)^2 + \frac{\Theta_0^2}{2}\left(\frac{\rho}{a}\right)^4\right) \tag{3.8}$$

$$B_\theta(\rho) = B_\phi(0)\left(\Theta_0\left(\frac{\rho}{a}\right) - \frac{\Theta_0^3}{2}\left(\frac{\rho}{a}\right)^3 + \frac{\Theta_0}{3}(\Theta_0^2 - 1)\left(\frac{\rho}{a}\right)^5\right) \tag{3.9}$$

where

$$\Theta_0 = \left[\frac{(6 - 6F)}{(3 - 2F)}\right]^{1/2} \tag{3.10}$$

Note that the shift corrected field profiles are in quite good agreement with the model profiles at this time in the discharge. The main difference is that our B_θ profile appears to be slightly higher in the central region and the B_ϕ profile somewhat narrower.

We recapitulate that these field profiles have been obtained by averaging over several shots and a time window of 60 μs. This means that they represent the equilibrium mean fields. The macroscopic dynamical behavior generally observed at these theta values has been smoothed out.

Having obtained the shift corrected coefficients for the polynomials it is now straightforward to proceed with the analysis using cylindrically symmetric equations.

3.2.4 Safety Factor

The safety factor profile can be calculated from the shift corrected field profiles from the expression:

$$q(\rho) = \frac{\rho}{R}\frac{B_\phi(\rho)}{B_\theta(\rho)} \tag{3.11}$$

written in cylindrical coordinates. The result is shown in fig.12. Already at this stage it is possible to draw some conclusions about what is to be expected from future fluctuation measurements in this parameter range. The safety factor profile appears to be

monotonically decreasing, thus we may not expect instabilities driven by pitch minima. The on axis value of the safety factor is q(0) ≈ 0.071. This means that resonant m=1 instabilities in the inner region of the plasma must have a toroidal mode number greater than | n | =14. Further more the q-value at the limiters is about q(a) ≈ - 0.03. We may therefore expect m=1 modes resonant outside the reversal surface to have toroidal mode numbers greater than | n | = 30.

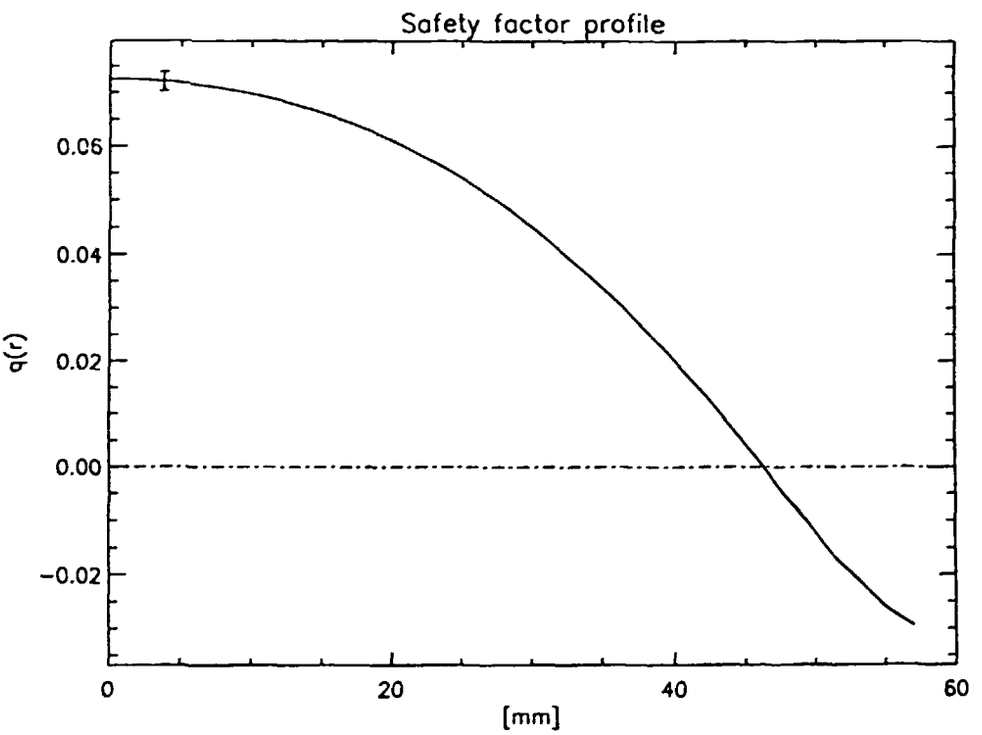

Fig.12. Safety factor profile

3.2.5. Current Densities

Following the cylindrical approximation the current density can be calculated according to Amperes law:

$$\mathbf{J} = \frac{1}{\mu_0} \nabla \times \mathbf{B} \qquad (3.12)$$

The expressions for the toroidal and poloidal current densities become in cylindrical coordinates

$$J_\phi = \frac{1}{\mu_0 \rho} \frac{d}{d\rho}(\rho B_\theta) \tag{3.13}$$

$$J_\theta = -\frac{1}{\mu_0} \frac{d}{d\rho}(B_\phi) \tag{3.14}$$

In fig.13 we show the poloidal and toroidal current densities calculated from the shift corrected field profiles in fig.11. The total toroidal plasma current, obtained by integrating the J_ϕ-profile, agrees within 2% of external Rogowski measurements.

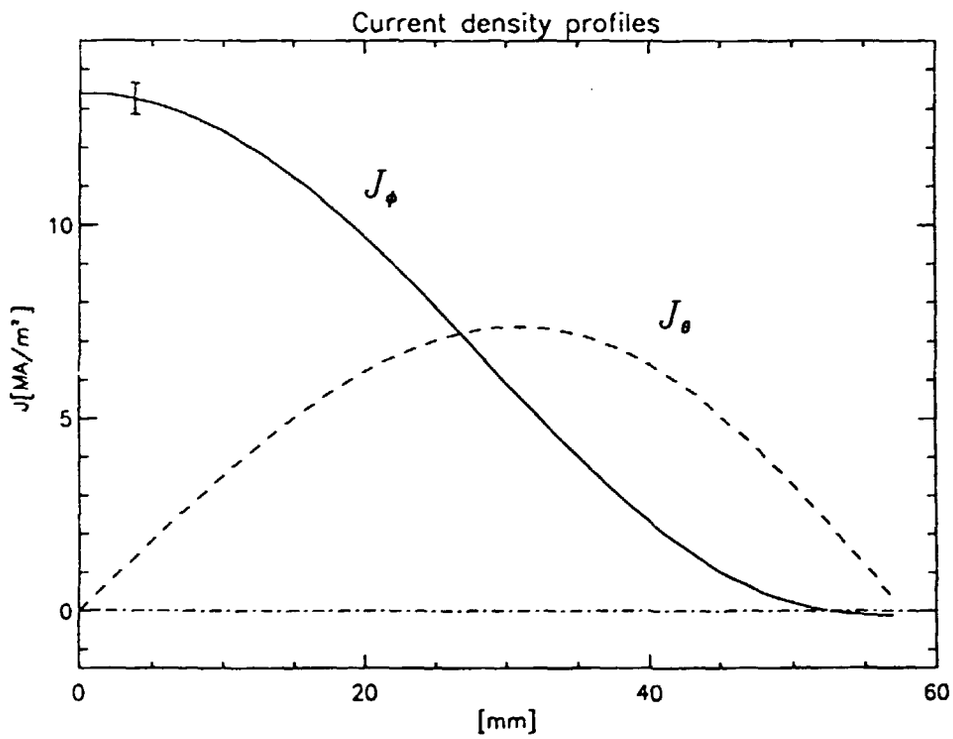

Fig.13. Current density profiles.

We observe that both J_ϕ and J_θ are approaching zero at the limiters with a slight reversal of J_ϕ near the limiters. Note that the current density is quite high, about 13 MA/m^2 on axis.

From the current densities and shift corrected field profiles we proceed to calculate the current density components parallel and perpendicular to the magnetic field. Upon normalizing with $B^2(\rho)$ and multiplying with μ_0, we obtain the so called μ-profile, which in the fully relaxed Taylor state is uniform across the plasma.

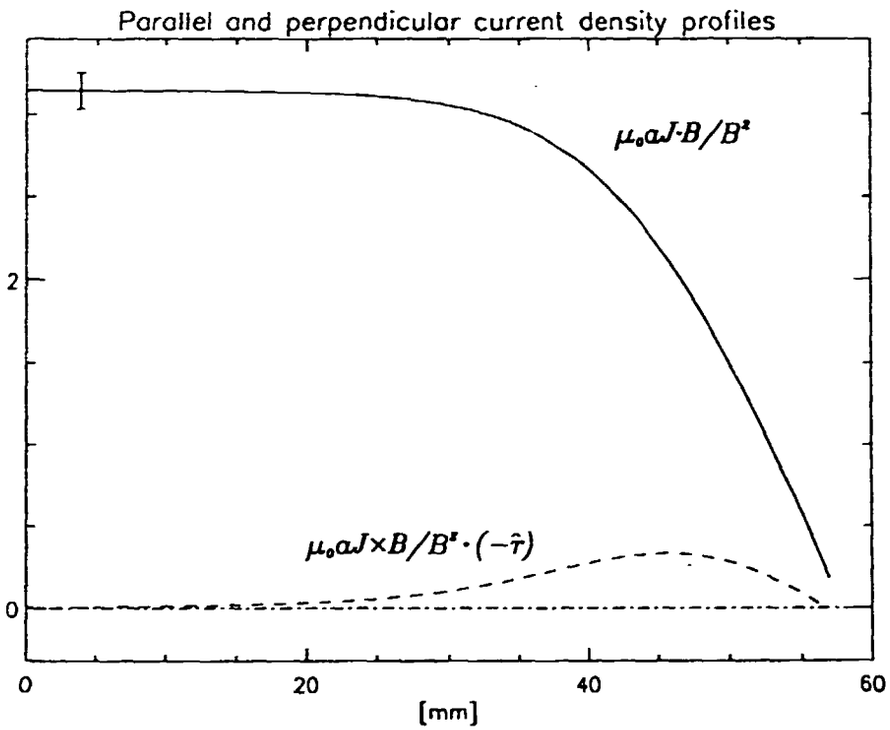

Fig.14. Profiles of parallel and perpendicular current densities.

We note that the discharge to a good approximation is force free. The current is flowing parallel to the magnetic field in the center of the discharge and the resulting μ-profile appears to be flat, or slightly peaked, out to about 70% of the minor radius. Then it decreases monotonically approaching zero at the wall. The perpendicular current density which is very small or zero in the center of the discharge shows a maximum just inside the reversal surface, telling us that the steepest pressure gradient is to be found in the edge region.

3.2.6. Pressure Profile and β-values

The pressure profile is obtained by assuming zero pressure at the boundary and integrating the equilibrium pressure balance equation:

$$\mathbf{J} \times \mathbf{B} = (J_\phi B_\theta - J_\theta B_\phi)(-\hat{r}) = \nabla P \qquad (3.15)$$

in cylindrical coordinates from the limiters inwards. As evident from this equation the pressure is directly related to the difference between the $J_\phi B_\theta$ and the $J_\theta B_\phi$ terms. In low β plasmas this difference is very small compared to the magnitude of the terms. This means that the computed pressure profile will be very sensitive to experimental errors in the magnetic field profiles. However, with the shift correction technique adopted in the computation of the field profiles, we are able to estimate the pressure profile with useful accuracy during the beginning of the sustainment phase where the best reproducibility is achieved. In fig.15 we show a pressure estimate obtained by averaging over ten discharges and a time window of 60 μs in the beginning of the sustainment phase. The pressure has been normalized to the on axis magnetic pressure.

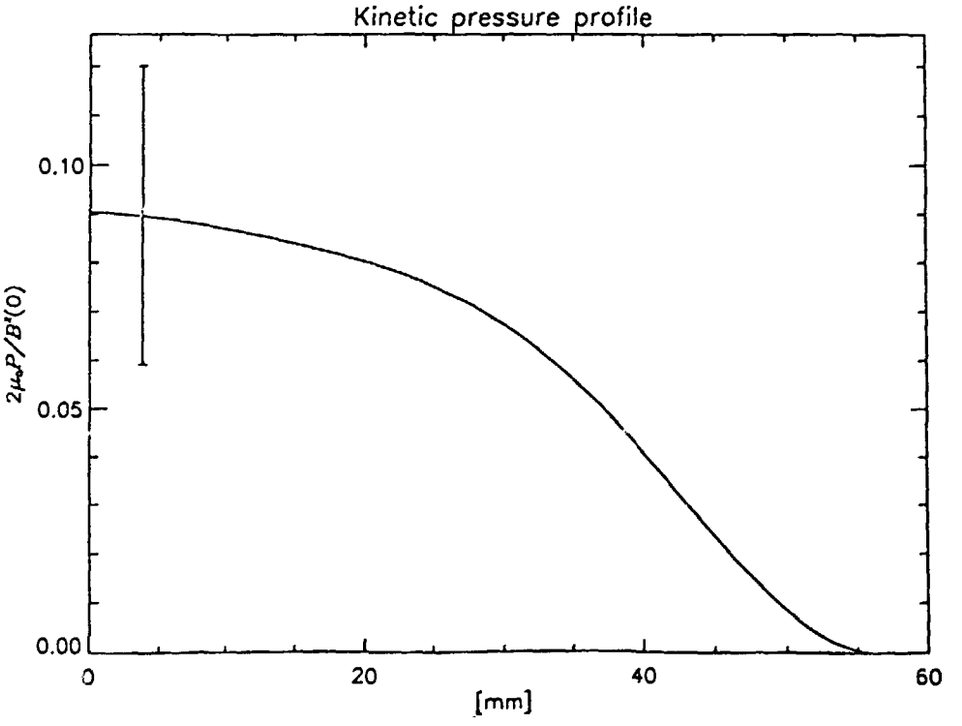

Fig.15. Plasma kinetic pressure, normalized to the on axis magnetic pressure.

The error bar shown in fig.15 pertains to the on axis pressure and is calculated from the propagation of systematical errors associated with the magnetic field measurements, as described in appendix A. The stochastic errors tend to cancel when averaging over several shots and time intervals. The standard deviation obtained from different orders of polynomial fits to the initial data fall within this range. Notice that the the cumulative uncertainty in the plasma center, indicated by the error bar, is rather large. The uncertainty varies approximately linearly to zero at the limiter radius because of the integration process.

The pressure profile appears to be slightly peaked in the central region, falling rapidly in the edge region approaching zero inside the limiters. Because of the uncertainty in the central region the detailed shape of the pressure profile is somewhat inconclusive. At the extreme of the estimated errors the profile may be anything from slightly hollow to rather peaked out to 30% of the limiter radius. The profile may be summarized in the following β-values:

$$\langle\beta\rangle = \frac{2\mu_0\langle p\rangle}{\langle B^2\rangle} = 0.09 \pm 0.03$$

$$\beta_\theta = \frac{2\mu_0\langle p\rangle}{B_\theta^2(a)} = 0.19 \pm 0.07$$

$$\beta_0 = \frac{2\mu_0 p(0)}{B^2(0)} = 0.09 \pm 0.03$$

As a confirmation of these results we note that at this time in the discharge, interferometer measurements show that the chord averaged electron density is about 10^{20} m^{-3}. The electron temperature obtained from line ratios of O^{+5} in the VUV region [7] is about 55 eV. Assuming a parabolic density profile for which $n_e(0) = 3/2\langle n_e\rangle$ and taking $T_i = T_e$, an independent rough estimate of the on axis beta-value can be calculated. The resulting estimate of the central beta becomes $\beta_0 = 0.091$ for $Z_{eff} = 1.5$ or $\beta_0 = 0.082$ for $Z_{eff} = 2.0$, which is in excellent agreement with the probe results.

3.3. Profile Dynamics

In this section the low frequency dynamical behavior of the equilibrium profiles will be presented. Here, instead of averaging over several shots, the time evolutions of single shots are studied. The data is smoothed to eliminate the high frequency fluctuation information. Then the discharge is divided into short time intervals (typically 2-5μs). The field profiles for each time interval are computed using the same shift correction technique as in the previous section. In this way we obtain a time series of shift corrected field profiles from which the dynamical evolution the equilibrium profiles can be computed.

It follows naturally from the limited number of data points over the radius, and the fact that we are not able to average over several shots without losing the details of the dynamics, that the time evolution studies are subject to larger errors than the long term equilibrium results. We also restate that we are not able to use the complementary edge coil data,without an accurate transfer function for the liner. This makes it extremely difficult to draw any conclusions of the time evolution of the pressure profile. Apart from the most sensitive result (the pressure) the results can be computed with useful accuracy.

3.3.1. Magnetic Fields

In fig.16 we show the time evolutions of the toroidal and and poloidal magnetic fields during the beginning of the sustainment phase of a typical RFP discharge. Notice that the fields are shift corrected so that each profile of B_θ and B_ϕ is expressed in terms of ρ originating at the magnetic axis.

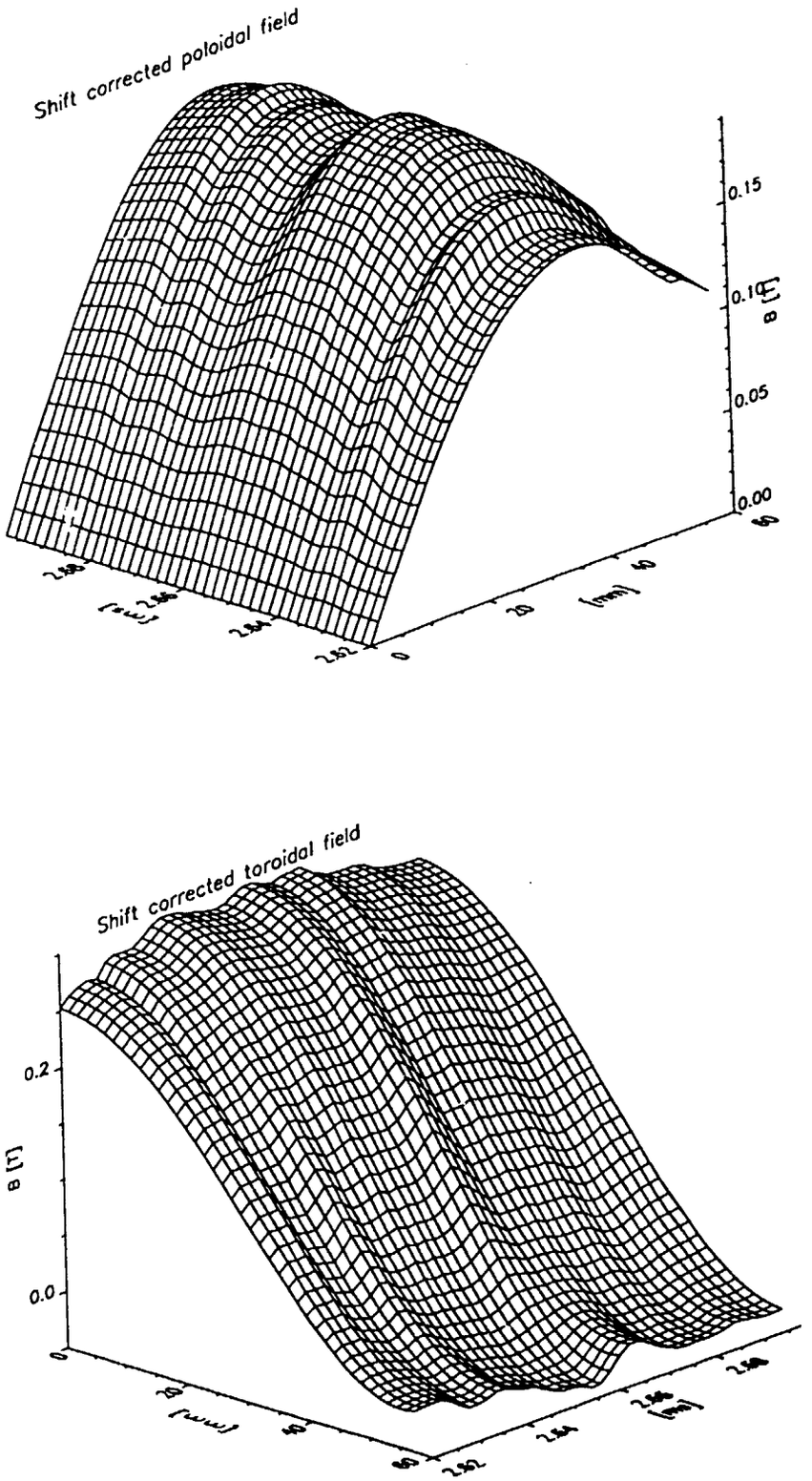

Fig.16. Time evolution of the magnetic field profiles

3.3.2. Safety Factor

We now proceed in a similar fashion and compute the time evolution of the safety factor profile, being plotted in fig.17.

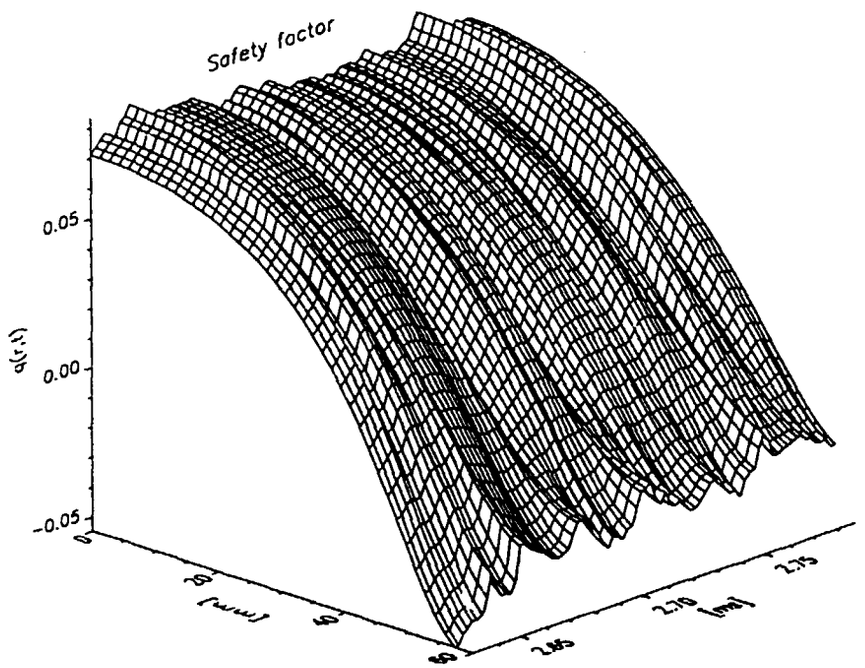

Fig.17. Time evolution of q-profile

In examining the details of the dynamical evolution of the q-profile we find that the safety factor tends to decrease in the central region with a simultaneous decrease in the reversed q(a), resulting in a flattening of the q-profile. This behavior is followed by a recovery of q(0) as well as q(a), restoring the shear in the configuration. This q-profile is taken for a $\Theta = 1.9$ shot. At lower Θ this apparently cyclic process is less obvious and the dynamics of the q-profile becomes quite irregular. At higher values of Θ sometimes oscillations with larger amplitude are seen.

3.3.3. Current Densities

In fig.18 we show the time evolution of the toroidal and poloidal current densities. Note that the current densities are fluctuating about zero at the wall, partly because in this case the edge coils could not be used to improve the edge fit.

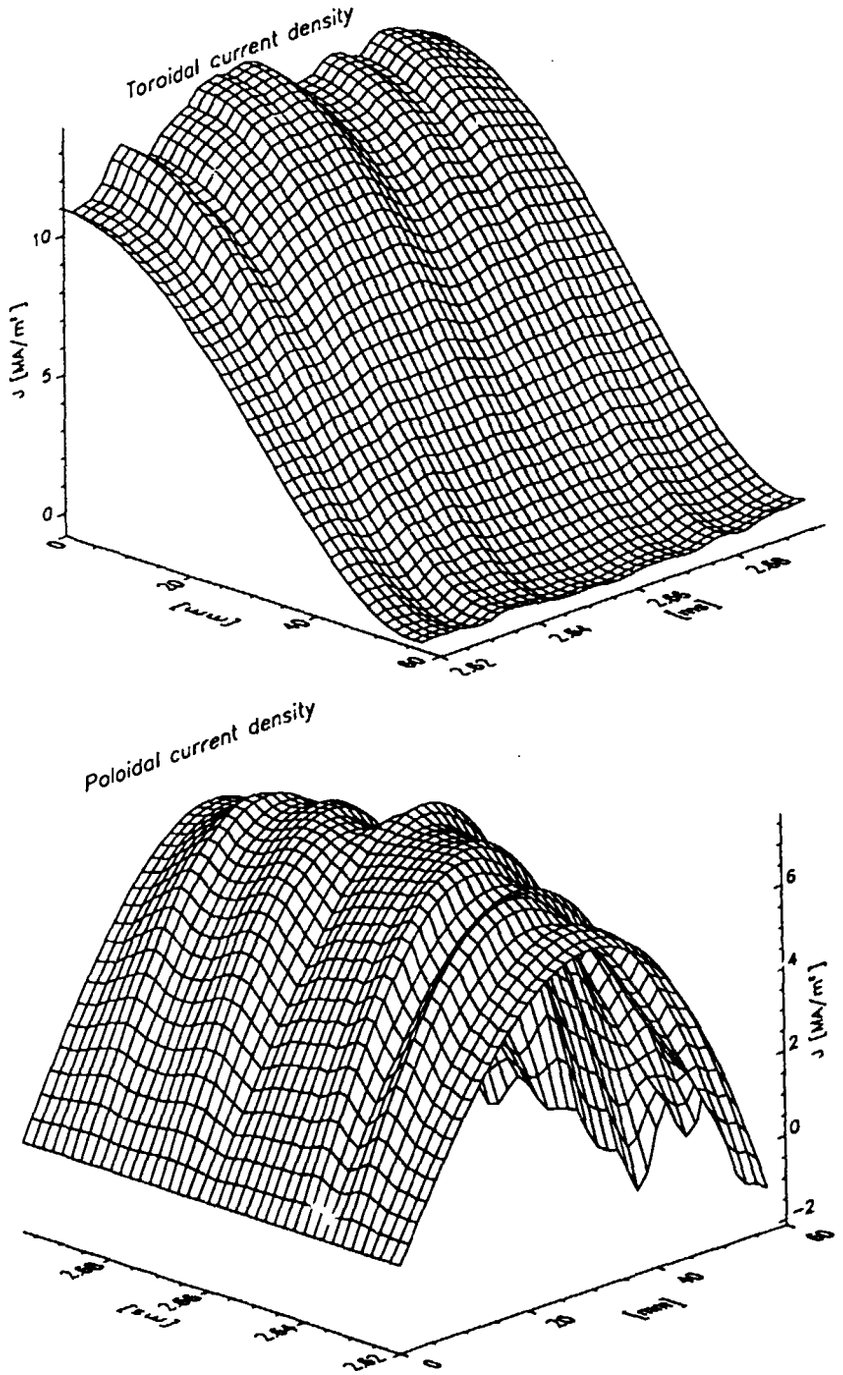

Fig.18. Time evolution of the current density profiles

3.3.4. μ-profile

Fig.19 shows the time evolution of the μ-profile during the beginning of the sustainment phase.

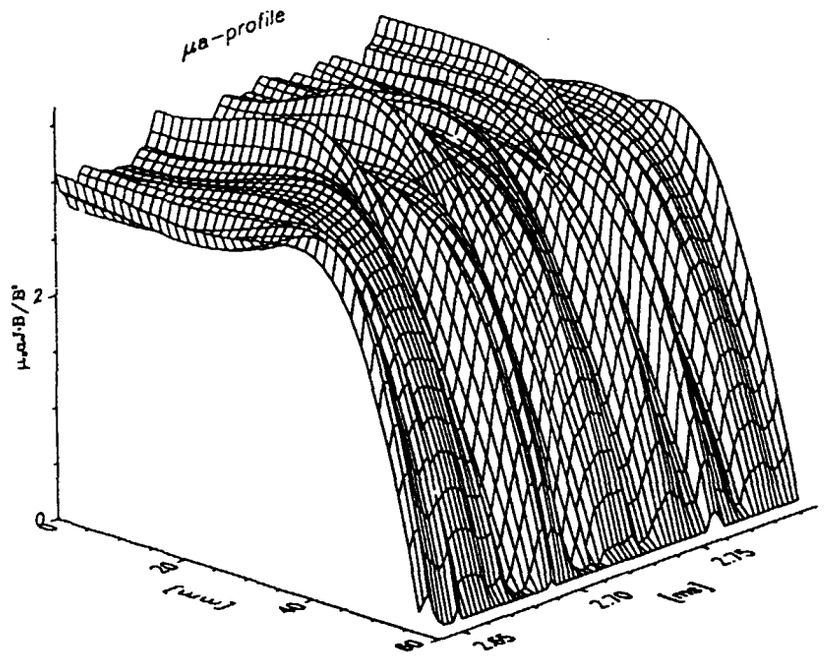

Fig.19. Time evolution of μ-profile

Upon a close inspection we observe that the μ-profile tends to peak on axis and then relax towards a flatter and broader shape. We are able to resolve a cyclic process where the toroidal current J_ϕ increases on axis thereby peaking the μ-profile, then J_ϕ is suppressed on axis while J_θ is increased in the edge region restoring a flatter and broader μ-profile. It is this macroscopic redistribution of the current in the plasma that give rise to the F-Θ oscillations which we showed in fig.6.

The probe discharges (fig.5.) may be characterized by a slightly decaying current and increasing V_{loop}/I_p. Towards the end of the discharge the parallel current density develops a hollow profile (fig.20.). This is resulting from a relative increase in the

poloidal current density in the edge region while the toroidal current density is suppressed in the central region.

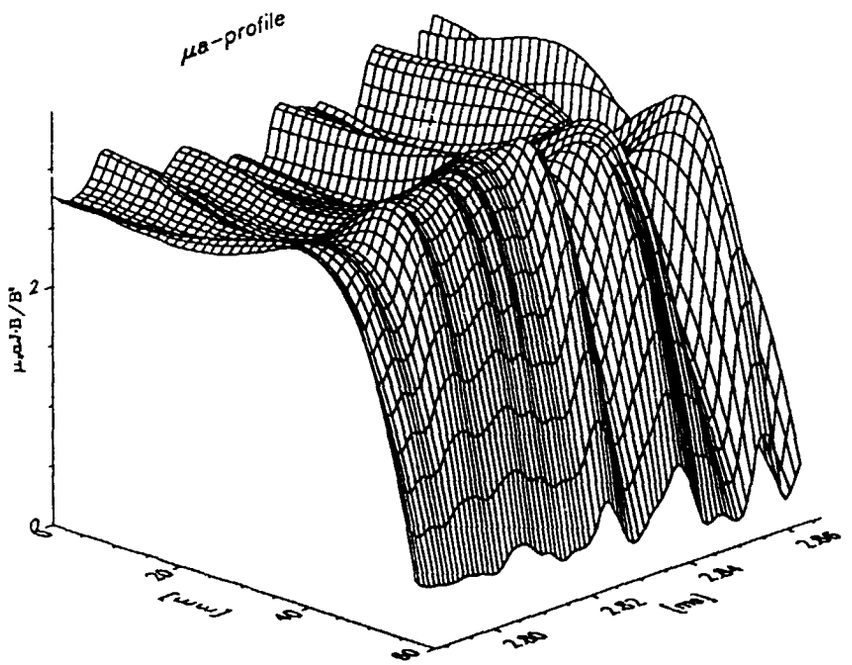

Fig.20. Towards the end of the discharge the μa - profile becomes broader and some times hollow.

3.3.5. Electric Fields

Inductive effects are of great importance in studying the dynamical behavior of the plasma. Since the probe measurements provides the evolution of the magnetic field with excellent time resolution, these effects can be computed rather directly on the basis of Faraday's law:

$$\nabla \times \mathbf{E} = - \frac{\partial \mathbf{B}}{\partial t} \qquad (3.14)$$

Applied to the cylindrical case the toroidal and poloidal electric field profiles to be determined from :

$$E_\phi(\rho) = E_\phi(a) - \int_\rho^a \frac{\partial B_\theta}{\partial t} d\rho \tag{3.15}$$

$$E_\theta(\rho) = -\frac{1}{\rho}\int_0^\rho \frac{\partial B_\phi}{\partial t} \rho d\rho \tag{3.16}$$

In fig.21 we show the profile of E_ϕ averaged over the sustainment phase. The boundary condition, i.e. the magnitude of the toroidal electric field at the wall, is provided by the loop voltage measurements. The peaking of the profile is an inductive effect due to the slightly decaying current.

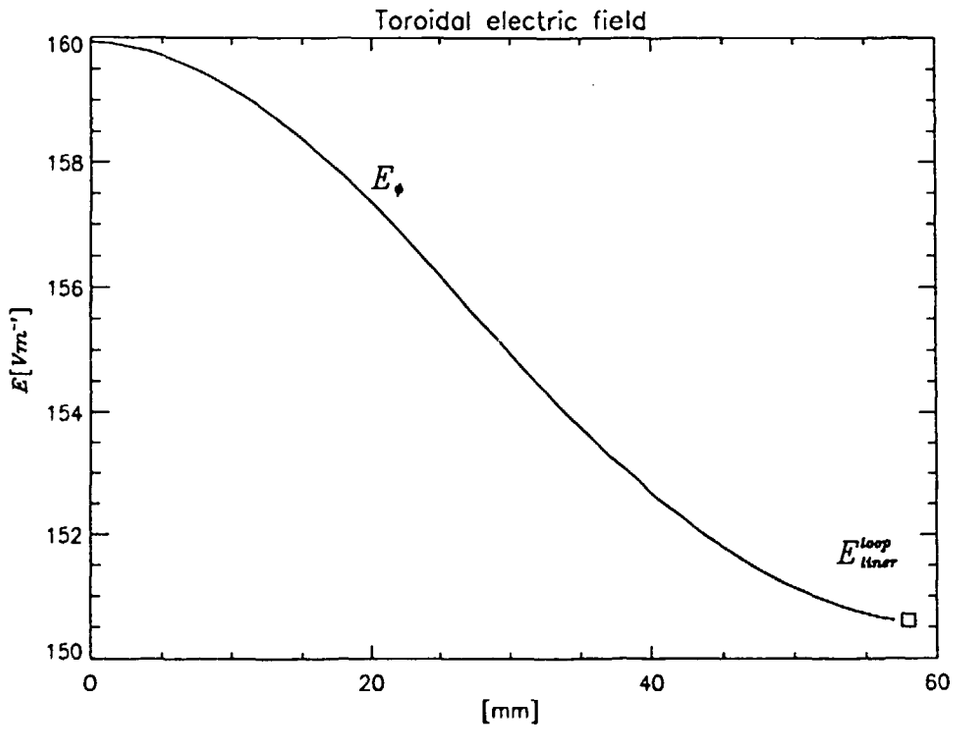

Fig.21. Toroidal electric field profile

The corresponding time averaged profile of the poloidal electric field, E_θ, is shown in fig.22. For this discharge the toroidal flux was approximately constant during the sustainment phase. For comparison we have included the time derivative of the toroidal flux calculated from an external flux loop. It can be seen that the external measurement is consistent with the probe data. We conclude that during this time period a redistribution of

the toroidal flux in the plasma occurs, ie. a broadening of the toroidal field profile. This is a common behavior towards the of the discharge as there is a relative increase in the poloidal current density in the edge region. This phenomenon is accompanied by an enhanced fluctuation level and an increase in Vloop/Ip.

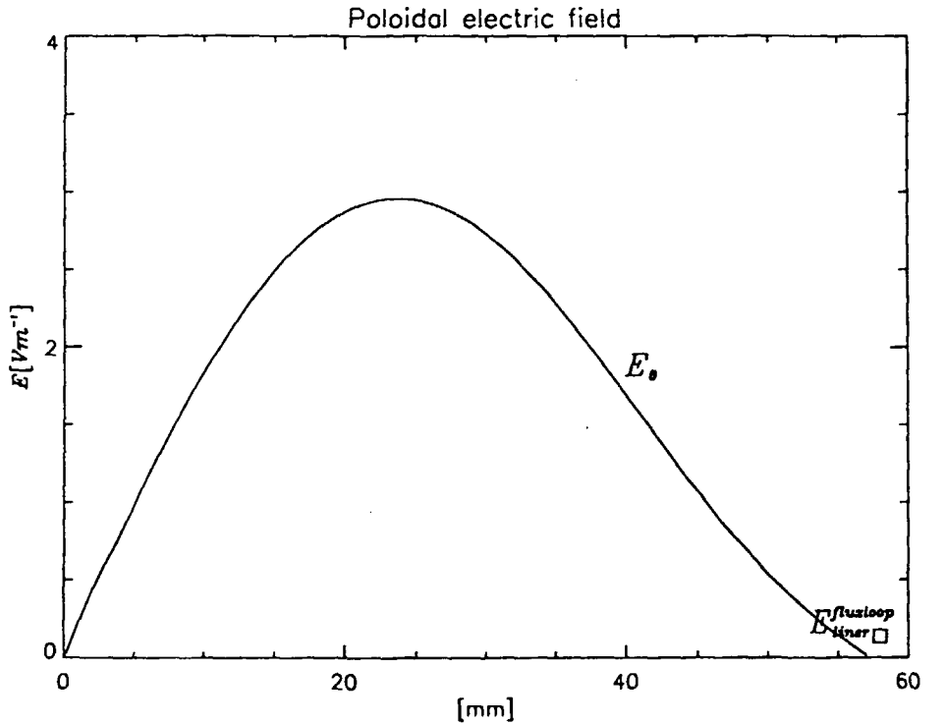

Fig.22. Poloidal electric field profile

In fig.23 we show the dynamical evolution of the inductive electric fields ($E_\phi(r)$ and $E_\theta(r)$) for a time slot during the sustainment phase. In section 3.3.7 we will show that these fields are not sufficient to drive the observed current densities.

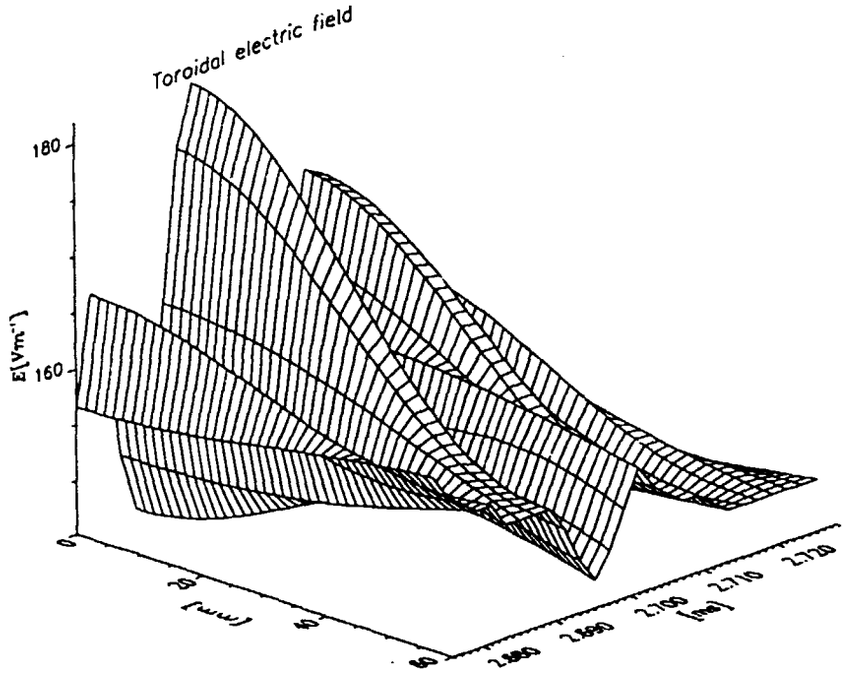

Fig.23.a. Time evolution of toroidal electric field

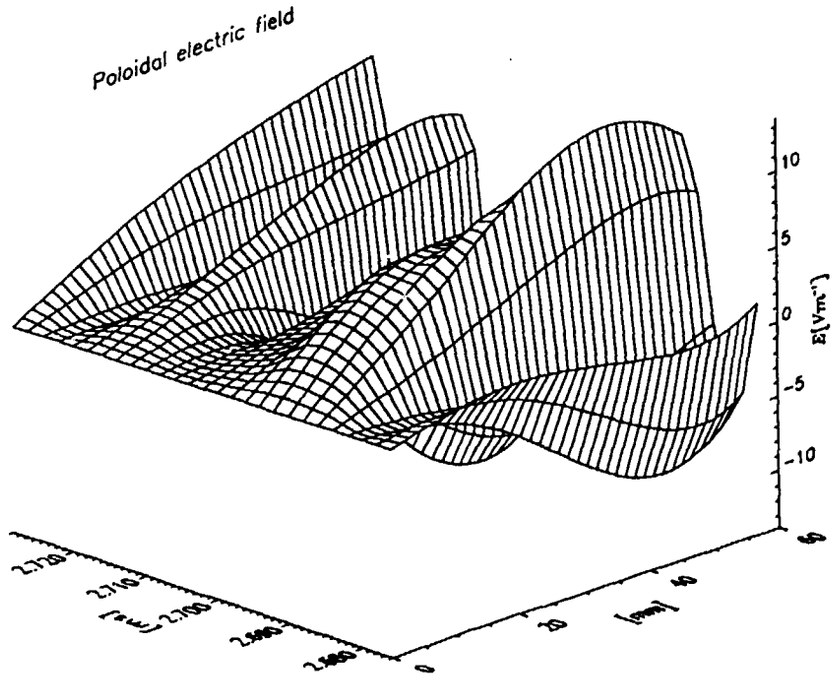

Fig.23.b. Time evolution of poloidal electric field

3.3.6. Power Input Density and Energy Confinement Time

Since we have obtained the profiles of **J** and **E**, it is now straight forward to calculate the power input density profile:

$$P_{in} = \mathbf{J}\cdot\mathbf{E} = J_\phi E_\phi + J_\theta E_\theta \tag{3.17}$$

The result is shown in fig.24.

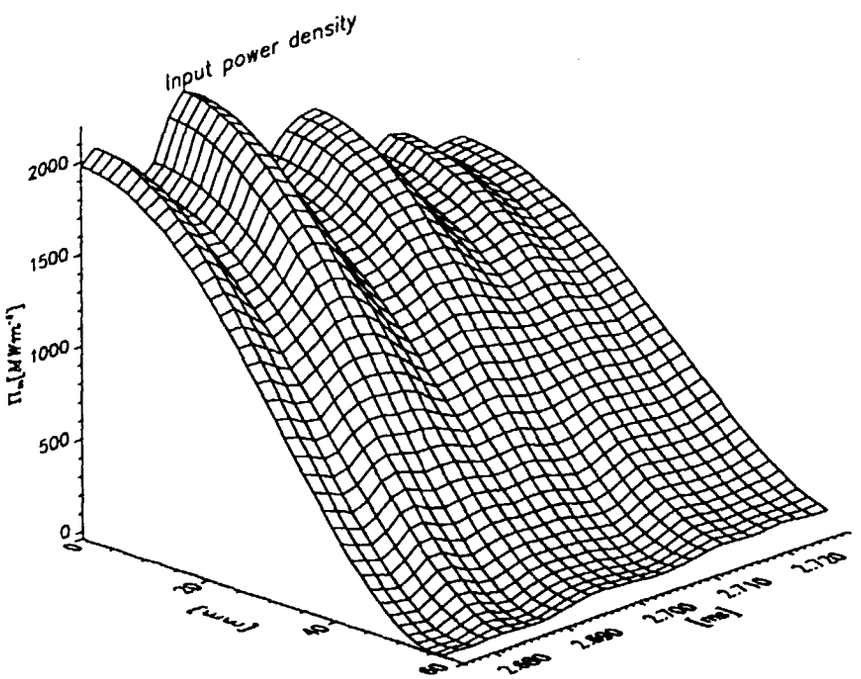

Fig.24. Input power density profile during sustainment phase

Note the rather rather high input power needed to sustain these discharges. This is mainly a consequence of T1-U being a small high aspect ratio machine, in particular with a small cross sectional area. However, it must be stressed that a significantly lower power input is sufficient in unperturbed discharges.

Having obtained the ohmic dissipation power profile, we are now in a position to make an estimation of the energy confinement time for these perturbed discharges. The plasma kinetic energy is calculated from the pressure estimates.

$$\tau_E = \int_{V_{plasma}} \frac{3}{2} P \, dV \Big/ \int_{V_{tot}} \mathbf{E} \cdot \mathbf{J} \, dV \qquad (3.18)$$

We arrive at an energy confinement time of $\tau_E = 5\ \mu s \pm 2\ \mu s$, where the uncertainty basically originates from the pressure estimates. The energy confinement time of unperturbed discharges, estimated under the assumptions of the independent pressure estimate discussed earlier, is about 10 μs.

3.3.7. Conductivity

From our equilibrium results we know that $J_{\parallel}$ is approximately an order of magnitude greater than $J_{\perp}$. This means that the magnetic field configuration is essentially determined by the parallel current density, $J_{\parallel} = \mathbf{J}\cdot\mathbf{B}/B$ (a very good approximation). We therefore now turn to the question of how the parallel current is driven. The effective parallel conductivity defined as:

$$\sigma_{\parallel} = \frac{\mathbf{J}\cdot\mathbf{B}}{\mathbf{E}\cdot\mathbf{B}} \qquad (3.19)$$

shows a strong "anomalous" behavior in RFPs. In fig.25. we plot $\sigma_{\parallel}$ obtained by averaging over the sustainment phase, where the inductive effects are small. For comparison we also include the Spitzer conductivity calculated from our pressure estimate, taking T_e = 55 eV on axis as indicated by spectroscopic measurements. The ion temperature is assumed to be equal to the electron temperature and the radial dependence of the temperature and density are assumed to be the same, i.e $T_e(r) \sim p(r)^{1/2}$. Spitzer estimates for $Z_{eff} = 2{,}4$ are plotted.

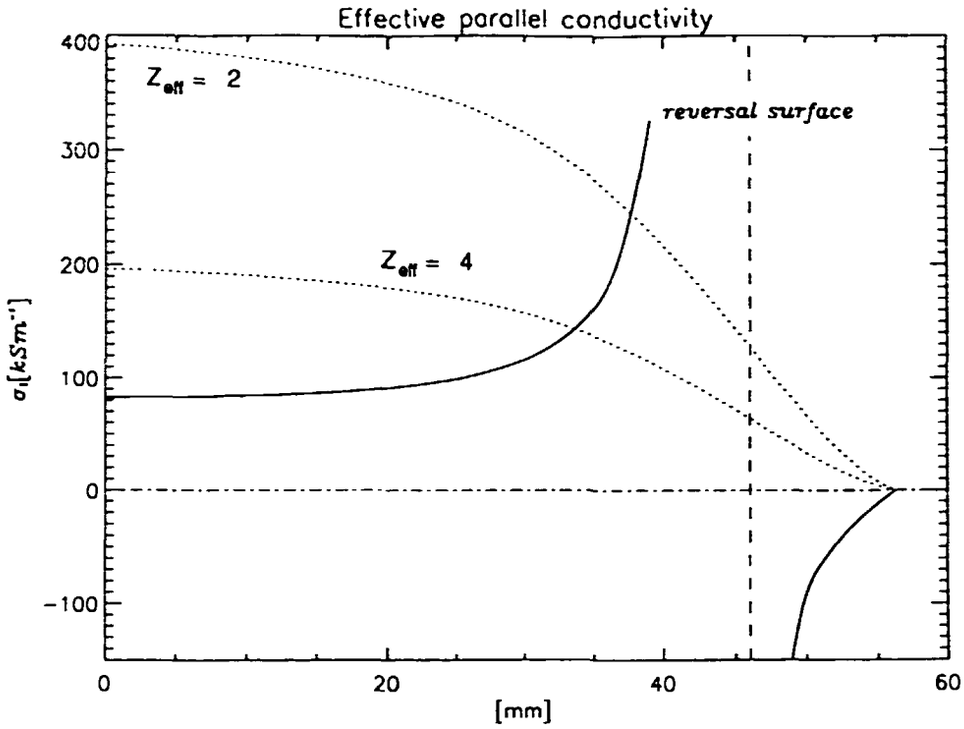

Fig. 25. Effective parallel conductivity profile (J·B)/(E·B). Spitzer estimates for Z_{eff} = 2,4 are plotted for comparison.

The profile of the current to field ratio is appearing hollow with a pole at the reversal surface, whereas the Spitzer estimate is monotonically decreasing. This contradiction can not be explained by assuming other physically realistic profiles of the temperature and density. There must exist a mechanism apart from the inductive electric fields which *suppresses the toroidal current density in the central region* and *drives poloidal current in the edge region.* This mechanism is often referred to as the "dynamo electric field".

4. DISCUSSION

In this paper we have presented a study of high current density RFP equilibria and profile dynamics in the EXTRAP T1-U machine. During the beginning of the sustainment phase we find that the mean profiles are in quite good agreement with the polynomial function model (PFM). The PFM is currently used for modeling the field profiles of unperturbed discharges on the T1-U experiment [11]. In PFM the profiles are expressed as simple functions of F and Θ. This is very convenient since these parameters are easily computed from external standard diagnostics. PFM estimates of helicity factor and inductance are in good agreement with probe data.

Substantial effort has been put into calibration and alignment of the probe and successful estimates of the pressure profile have been obtained in the sustainment phase of the discharge. As we have pointed out the pressure estimate is very sensitive to experimental errors. Nevertheless, the resulting central beta agrees well within the estimated errors with independent measurements of the central pressure. The β-values we obtain seem to be somewhat higher than commonly observed on other RFP experiments. The reason might be the relatively high electron densities obtained in T1-U. High values of β_θ (20% to 30%) have also been obtained in the OHTE reversed field pinch [1], which similar to T1-U is a high aspect ratio device.

In the fully relaxed minimum energy state described by Taylor [12] [13] the spatial function μ is uniform across the plasma, and the field profiles are described by the bessel function model (BFM). The resulting force free Taylor F-Θ curve was plotted for reference in figure 6. Note that the discharges tend to evolve to an F-Θ locus slightly above the BFM in the neighborhood of the PFM curve. Experimentally μ is found to be (as in our case) non uniform and decrease to zero at the wall. None uniform μ-profiles has also been measured in OHTE, HBTX-1A, ETA-BETA II, ZT-40M and REPUTE [1-6]. The difference between the experimentally observed μ-profiles and the theoretically uniform μ-profile depends on the presence of pressure and temperature gradients near the

wall. In the high temperature central region where the pressure gradient is small, the μ-distribution is close to uniform, but in the outer resistive edge region there is generally less current flow than would correspond to the fully relaxed state.

Although Taylors theory elegantly points out the existence of a minimum energy state with reversed toroidal field (BFM), it says nothing about the relaxation process or about the sustainment of laboratory RFPs well beyond the resistive diffusion time. Experimentally it is a well known fact that supplying volt seconds for the poloidal flux sustains also the toroidal magnetic field configuration. RFPs are characterized by a relatively high level of fluctuations. Although the mechanism is not well understood at the present time these fluctuations tend to restore a close to uniform μ-distribution and thereby, while sustaining the configuration against diffusion, keeping the discharge in the neighborhood of the relaxed state. It has been pointed out [14] that the sustainment of RFPs may be interpreted as a dynamic balance between heating and diffusion on the one hand and magnetic relaxation on the other. The former tend to create a peaked μ-distribution which destabilize the configuration, while the latter acts to restore a flatter and more stable μ-profile. The fluctuations involved in this process are commonly referred to as MHD activity. At low Θ this activity forms a low level turbulent background from which it is possible to find average coherence properties by statistical means only. However, in high Θ discharges global periodic disturbances are often seen on several plasma signals.

In this paper we have presented results from Extrap T1-U showing that, in the regime of $\Theta \approx 1.8$, it is indeed possible to resolve a cyclic process where the parallel current density tends to peak in the central region and then relax towards a flatter and broader configuration. In other words the current channel narrows as the toroidal current density (J_ϕ) in the central region increases, followed by a suppression of J_ϕ on axis and an increase in J_θ in the edge region. The process appears to repeat it self in a cyclic manner. These observations are consistent with insertable magnetic probe measurements on REPUTE and ETA-BETA II [5] [6]. However, in these machines generally larger amplitudes in the oscillations are observed at this Θ-value. In our case giant oscillations

are only sporadically seen at these Θ and they seem to appear more often in ramped discharges. No systematic scan of the pinch parameter has been done at this time.

Another interesting observation is that the parallel current density tends to develop a hollow profile towards the end of the discharge. The toroidal current density is strongly suppressed in the central region, while there is a relative increase in the poloidal current density in the edge region. We find that this phenomenon is accompanied by an enhanced fluctuation level and a gradual increase in Vloop/Ip (a behavior not observed in unperturbed discharges, except during the termination phase). This type of hollow μ-profiles have been observed recently [15] in in non linear 3D resistive MHD simulations for the case of resistive and distant shells. The cause of this behavior might be that the plasma responds by stronger relaxation, as insertion of the probe generally increases the dissipation rate for the system.

5. CONCLUSIONS

The structure of the reversed field pinch equilibrium and the time evolution of the profiles have been studied during high current density discharges in EXTRAP T1-Upgrade. When the probe was inserted there was a somewhat shorter pulse duration and a an increase in the power input needed to sustain the discharge. The quantitative appearance of reversal ratio and pinch parameter where similar to unperturbed discharges. VUV spectroscopy indicated burn through of low Z impurities. The electron temperature was about 55 eV.

Measurements of the plasma displacement show essentially a uniformly shifted equilibrium. Accordingly the field profiles may be corrected for a uniform perpendicular shift. During the beginning of the sustainment phase, where the best reproducibility is achieved, the mean field profiles are found to be in quite good agreement with a PFM description.

The current densities are found to be quite high, typically 13 MA/m^2 on axis. Examining profiles of the safety factor we find that we may not expect instabilities driven by pitch minima. In addition, modes resonant inside the reversal surface would have $|n| > 14$, while externally resonant modes would have $|n| > 30$.

Considerable effort was put into the determination of the pressure profile and the results agrees within the estimated errors with independent measurements of electron temperature and density. The pressure profile appears to be slightly peaked in the central region, falling more steeply in the edge region. Values of $\langle\beta\rangle \approx 9\%$ and $\beta_\theta \approx 19\%$ are found leading to an estimation of the energy confinement time of $\tau_E \approx 5\ \mu s$, with the probe inserted.

Profiles of the effective parallel conductivity have been computed and compared to Spitzer estimates calculated from our pressure profile. The difference cannot be explained by assuming realistic temperature and density profiles. This result clearly indicates the presence of a "dynamo" mechanism sustaining the field configuration.

The probe discharges tend to evolve to relatively deeply reversed high Θ discharges. In such discharges macroscopic F-Θ oscillations are often observed by edge diagnostics. We find that these oscillations represent macroscopic redistributions of the current in the plasma. A dynamic process is found where the parallel current density tends to peak in the central region and then relax towards a flatter and broader configuration. Towards the end of the discharge there is an increasing fluctuation level along with an increasing V_{loop}/I_P. Here we find a relative increase in the poloidal current density in the edge region resulting in a hollow μ-profile. This behavior is often followed by a disruptive termination of the discharge.

ACKNOWLEDGEMENTS

The authors whish to thank Dr. E. Tennfors and Dr. J. Scheffel for valuable comments on the manuscript. We also would like to thank K-D. Zastrow for fruitful discussions and for providing the spectroscopic data. Furthermore we would like to thank the technical and engineering staff of the Department of Fusion Plasma Physics for their help and support.

This work has been supported by the European Communities under an association contract between Euratom and Sweden.

REFERENCES

[1] TAMANO T., CARLSTROM T.N., CHU C., et al., in Plasma Physics and Controlled Nuclear Fusion Research 1982 (Proc. 9th Int. Conf. Baltimore, 1982), Vol. 1, IAEA,Vienna (1983) 609.

[2] ANTONI V., MARTINI S., ORTOLANI S., PACCAGNELLA R., in Mirror-Based and Field-reversed Approaches to Magnetic Fusion (Proc. Course Varenna, 1983), Vol. 3, Int. School of Plasma Physics, Varenna (1984) 107.Plasma Phys.

[3] ASAKURA N., FUJISAWA A., FUJITA T, et al., in Plasma Physics and Controlled Nuclear Fusion Research 1986 (Proc. 11th Int. Conf. Kyoto, 1986), Vol. 2, IAEA,Vienna (1987) 433.

[4] HOWELL R.B., INGRAHAM J. C., BURKHARDT E.J., NILLES, E.J., YOSHIDA Z.,Bull. Am. Phys. Soc. **31** (1986) 1547.

[5] UEDA Y., ASAKURA N., MATSUZUKA S., YAMAGISHI K., et al., Nuclear Fusion **27** (1987) 1759.

[6] ANTONI V., MARTIN P., ORTOLANI S., Nuclear Fusion **29** (1989) 1759.

[7] ZASTROW K.D., BRZOZOWSKI J.H., KÄLLNE E., SUMMERS H.P. ,Workshop on Diagnostics for Contemporary Fusion Experiments, Varenna, 1991.

[8] BRUNSELL P., BRYNOLF J., HELLBLOM G., Report TRITA-ALF-92-01, Royal Institute of Technology, Stockholm 1992.

[9] BROTHERTON-RATCLIFFE D., HUTCHINSON I.H., Culham Report CLM-R246 (1984).

[10] SPROTT J.C., Phys. Fluids **31** (1988) 2266.

[11] MAZUR S., NORDLUND P., DRAKE J.R., Report TRITA-PFU-90-09, Royal Institute of Technology, Stockholm 1990.

[12] TAYLOR J.B., Phys. Rev. Lett. **33** (1974) 1139.

[13] TAYLOR J.B., Rev. Mod, Phys., **58** (1986) 741.

[14] ORTOLANI S., 16th European Conference on Controlled Fusion and Plasma Physics, Venice 1989.

[15] SCHNACK D.D., ORTOLANI S., Nuclear Fusion **30** (1990) 227.

APPENDIX A

ERROR PROPAGATION ANALYSIS

As described in section 2.2.2 the systematical errors could, by means of careful calibration and alignment, be limited to 4%. By collecting data with the probe positioned at different radii, the effect of these systematical errors can be reduced. The statistical errors tend to diminish when fitting the polynomials to several shots averaged over a time window.

The error propagation analysis, described in this appendix, is performed for the same set of raw data as in fig.7, i.e. a series of ten discharges where the probe has been shifted 5 mm radially to obtain 16 radial measurements of the magnetic field. The method used is to perturb the coefficients in the calibration matrix with an error corresponding to the estimated maximum systematical error and perform the analysis with the perturbed calibration matrix. In this way the results derived from the perturbed matrix can be compared with the unperturbed results to show how a systematical error in the calibration matrix propagates to the different calculated quantities. Each element in the calibration matrix is perturbed with a random error, uniformly distributed between -4% and +4%. Analysis is performed for the data, from the series of ten shots averaged over 60 μs, using both the unperturbed matrix and ten different matrixes perturbed with a 4% error. The results are shown in figs. A1-A5 . The solid curves represent the results from the initial unperturbed calibration matrix, whereas the results from the perturbed matrixes are shown with dashed curves. The resulting errors are calculated as the standard deviation from the best estimates.

$$\sigma = \sqrt{\frac{1}{N-1}\sum_{p=1}^{10}(x_p - x_u)^2} \qquad (A.1)$$

Where x_p and x_u represents the unperturbed and perturbed quantities respectively.

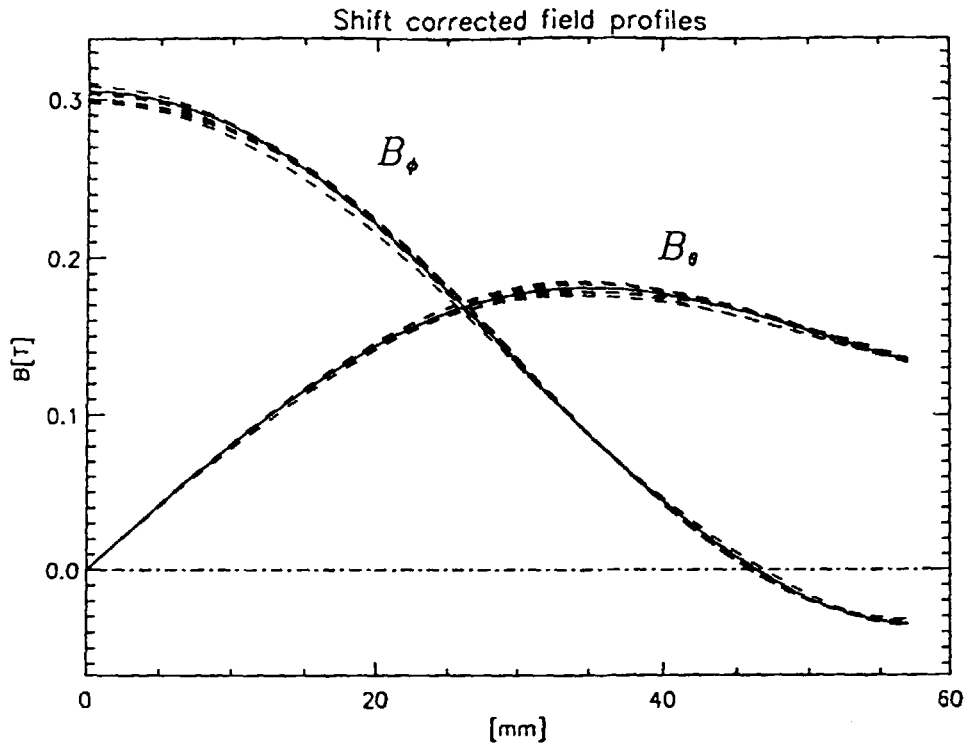

Fig. A1. Shift corrected magnetic field profiles, $\sigma = \pm 1.5$ %.

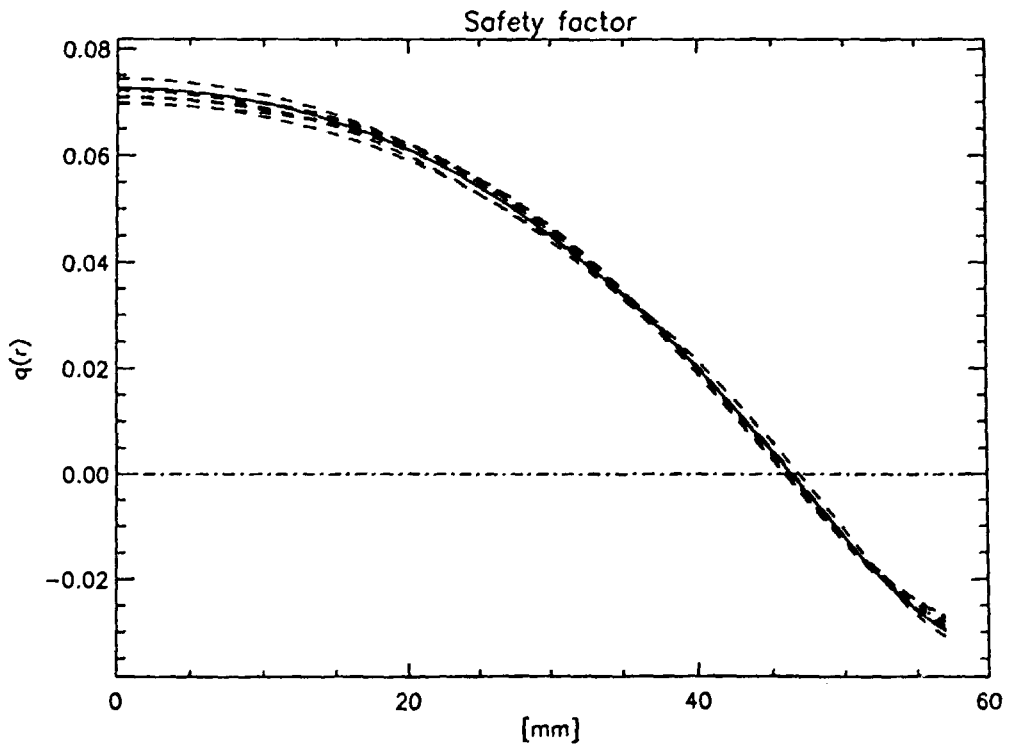

Fig. A2. Safety factor, $\sigma = \pm 2.5$ %.

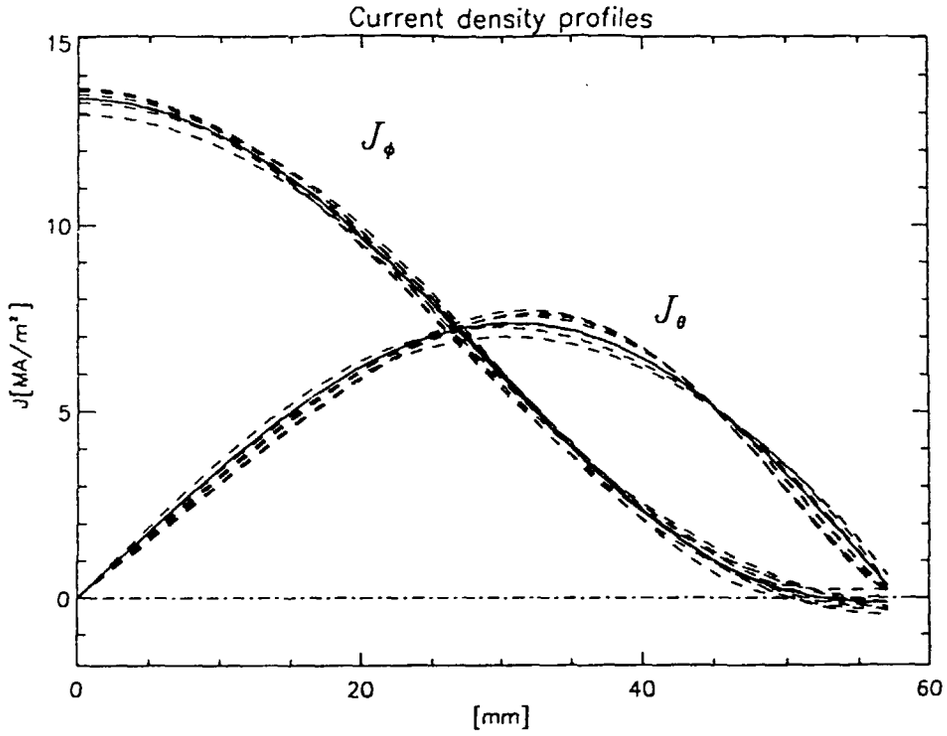

Fig. A3. Current densities, $\sigma = \pm 3$ %.

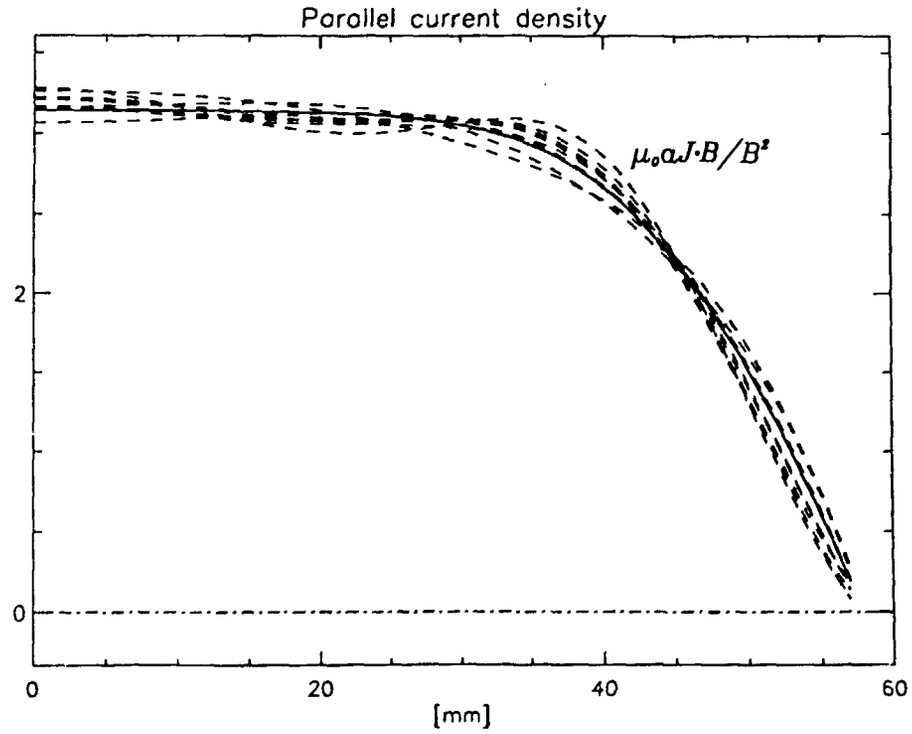

Fig. A4. μa-profile, $\sigma = \pm 3.5$ %.

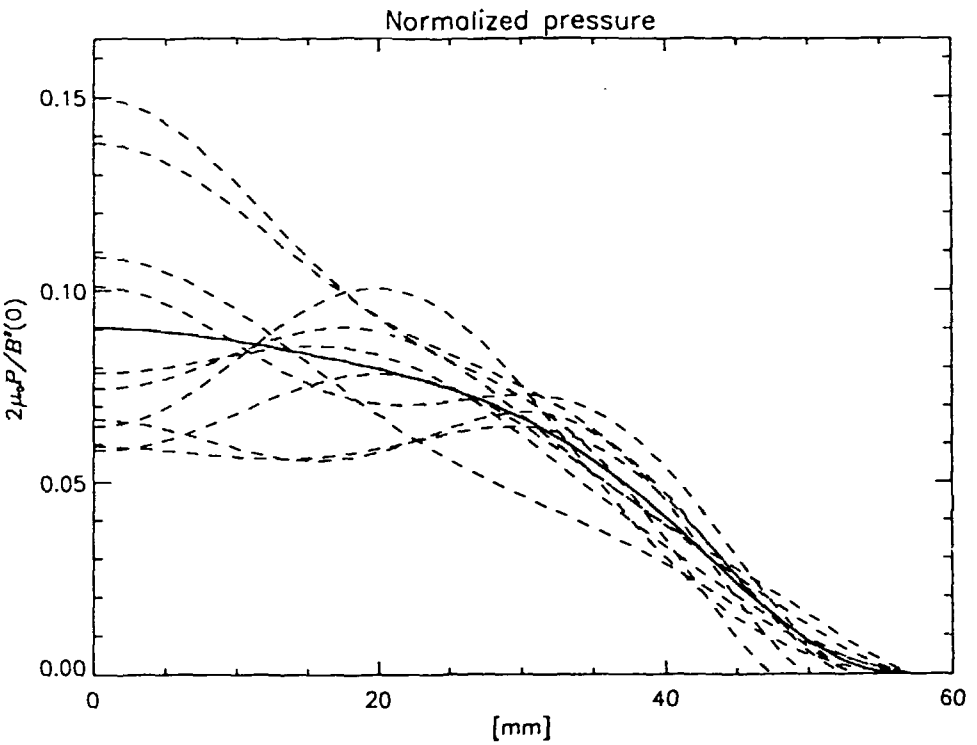

Fig. A5. Pressure, $\sigma = \pm 34$ %.

Note that the uncertainty in the on axis pressure is rather large (about 34%). This is due to the accumulation of errors in the integration process.

APPENDIX B

CORRECTION OF THE FIELD PROFILES FOR A UNIFORM PERPENDICULAR SHIFT

We here outline the derivation of a method to correct the field profiles for a uniform perpendicular (with respect to the probe) shift. This technique was originally developed for vertically inserted probes on the HBTX-1A reversed field pinch. [9], where (in contrast to our results) it was found that the parallel shift could be neglected. As a starting point for this derivation we shall assume that the parallel shift has been properly corrected for as described in section 3.2.2. From 3.2.2 we also recapitulate that, after correcting for the parallel shift, the equilibrium may be characterized by a set of concentric flux surfaces whose center is displaced a distance $\Delta_\perp$ perpendicular to the probe. We now introduce a Cartesian coordinate system with the y-axis along the probe. The measured toroidal and poloidal fields will be referred to as $B_z^m(y)$ and $B_x^m(y)$ respectively. The question addressed is to determine $B_z(\rho)$ and $B_\varphi(\rho)$, where ρ is a cylindrical coordinate originating at the magnetic axis.

B.1 Toroidal Field

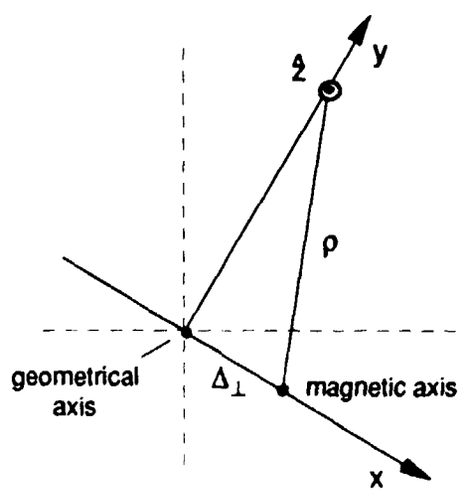

Fig.B1

From fig.B1 it is evident that :

$$B_z(\rho) = B_z(\sqrt{y^2+\Delta_\perp^2}) \tag{B.1}$$

Now, if $\Delta_\perp^2 / y^2 << 1$ we may expand :

$$y\left(1+\frac{\Delta_\perp^2}{y^2}\right)^{1/2} \approx y+\frac{\Delta_\perp^2}{2y} \tag{B.2}$$

accordingly :

$$B_z(\rho) \approx B_z\,(y+\frac{\Delta_\perp^2}{2y}) \tag{B.3}$$

We now Taylor expand about y :

$$B_z(\rho) \approx B_z(y)+\frac{\Delta_\perp^2 dB_z}{2y\ d\rho} \tag{B.4}$$

By definition (fig.B1) :

$$B_z(\rho) = B_z^m(y) \tag{B.5}$$

B.4 and B.5 may be combined to give:

$$B_z(y) \approx B_z^m(y) - \frac{\Delta_\perp^2}{2y}\frac{dB_z^m}{dy} \tag{B.6}$$

which is valid provided $\Delta_\perp^2 / y^2 << 1$. Obviously eq. B.6 is not valid near y = 0. Here we must use a Maclaurin expansion. We have:

$$B_z(\rho) \approx B_z(0) + \frac{\rho^2}{2}\left[\frac{d^2B_z}{d\rho^2}\right]_{\rho=0} \tag{B.7}$$

In this region (where $y \rightarrow 0$) $\rho \approx \Delta_\perp$. Hence, we may rewrite B.7 as:

$$B_z(\rho) \approx B_z(y) + \frac{\Delta_\perp^2}{2}\left[\frac{d^2B_z^m}{dy^2}\right]_{y=0} \qquad (B.8)$$

Since near the axis

$$\left[\frac{d^2B_z^m}{dy^2}\right]_{y=0} \approx \frac{1}{y}\frac{dB_z^m}{dy} \qquad (B.9)$$

we again obtain eq. B.6. We therefor conclude that the proper correction formula for B_z is:

$$B_z(y) \approx B_z^m(y) - \frac{\Delta_\perp^2}{2y}\frac{dB_z^m}{dy} \qquad (B.10)$$

Accordingly, if B_z^m is expanded as an even polynomial series in y :

$$B_z^m(y) = \sum_{j=0}^{n} b_j y^{2j} \qquad (B.11)$$

the corrected field may be written :

$$B_z(y) = \sum_{j=0}^{n} b_j (1 - \frac{j\Delta_\perp^2}{y^2}) y^{2j} \qquad (B.12)$$

B.2 Poloidal Field

In a similar way a shift correction formula for the poloidal field component may be derived.

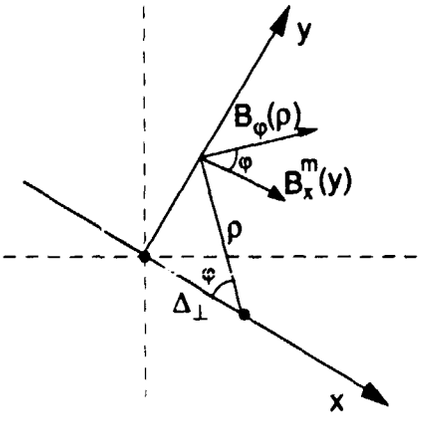

Fig.B2

From fig.B.2 it can be seen that :

$$\frac{B_x^m(y)}{y} = \frac{B_\varphi(\rho)}{\rho} \tag{B.13}$$

We now proceed as above. Expansions near the axis and in the outer region results in the formula :

$$B_\varphi(y) = B_x^m(y) - \frac{\Delta_\perp^2}{2} \frac{d}{dy}\left(\frac{B_x^m}{y}\right) \tag{B.14}$$

ie.if B_x^m is expended as an odd polynomial series in y :

$$B_x^m(y) = \sum_{j=0}^{n} a_j\, y^{(2j+1)} \tag{B.15}$$

the corrected field is obtained from :

$$B_\varphi(y) = \sum_{j=0}^{n} a_j \left(1 - \frac{j\Delta_\perp^2}{y^2}\right) y^{(2j+1)} \tag{B.16}$$

After correcting for $\Delta_\perp$ the coordinate y along the probe may be replaced by the cylindrical coordinate ρ originating at the plasma axis.

TRITA-ALF-92-03
Department of Fusion Plasma Physics
Alfvén Laboratory, Royal Institute of Technology,
S-100 44 STOCKHOLM,Sweden

Reversed Field Pinch Magnetic Equilibrium and Profile Dynamics in Extrap T1-Upgrade

P. Nordlund , S. Mazur and J.R. Drake

54 pages, in English

Abstract

An eight station insertable magnetic probe has been installed on the Extrap T1-U machine. The structure of the Reversed Field Pinch magnetic equilibrium and the time evolution of the profiles has been studied. The probe was inserted into sustained high current density RFP plasmas, typically 12-16 MA/m^2 on axis. When the probe was inserted there was a somewhat shorter pulse duration and a slightly decaying current. The magnetic field profiles are shift corrected and expressed in a cylindrically symmetric form. All quantities are then derived from cylindrically symmetric equations.

In the beginning of the sustainment phase, where the best reproducibility is achieved, we have been able to obtain estimates of the pressure profile consistent with independent measurements of the central pressure. Values of $\beta_\theta \approx 0.19$ and $< \beta > \approx 0.09$ are found leading to an estimation of the energy confinement time, with the probe inserted, of $\tau_E \approx 5$ μs.

Profiles of the effective parallel conductivity clearly indicates the presence of a "dynamo mechanism" sustaining the field configuration. High Θ discharges usually exhibit large oscillations in the F-Θ plane. We find that these oscillations represents macroscopic redistribution of the current in the plasma. A cyclic process is found where the parallel current density (μ–profile) tends to peak in the center and then relax towards a flatter and broader configuration. Towards the end of the discharge there is an increasing fluctuation level along with an increasing V_{loop}/ I_p. Here we find a relative increase in the current density in the edge region resulting in a hollow μ–profile.

Key words: Reversed Field Pinch (RFP), Extrap T1, magnetic probe, magnetic field profiles, profile dynamics